JGR Biogeosciences

RESEARCH ARTICLE
10.1029/2025JG009132

Controls on brGDGT Production in the Seasonally Anoxic Water Column and Sediments of Rotsee (Lake Rot)

Fatemeh Ajallooeian[1,2], Nathalie Dubois[1,3], S. Nemiah Ladd[4], Mark Alexander Lever[5,6], Carsten Johnny Schubert[5,7], and Cindy De Jonge[1]

[1]Department of Earth and Planetary Sciences, Geological Institute, Zurich, Switzerland, [2]Department of Earth Sciences, University of Oxford, Oxford, UK, [3]Swiss Federal Institute of Aquatic Science and Technology, Dubendorf, Switzerland, [4]Department of Environmental Science, University of Basel, Basel, Switzerland, [5]Institute of Biogeochemistry and Pollutant Dynamics, ETH Zurich, Universtitätstrasse 16, Zürich, Switzerland, [6]Marine Science Institute, University of Texas at Austin, Port Aransas, TX, USA, [7]Swiss Federal Institute of Aquatic Science and Technology, Kastanienbaum, Switzerland

Key Points:

- MBT'_{5ME} values in Rotsee are influenced by lake stratification while the isomer ratio (IR) more directly reflects epilimnion temperature
- MBT'_{5ME} and IR are strongly correlated, providing a diagnostic framework to identify sedimentary brGDGTs that originate from surface waters
- Multiple bacterial groups, not just Acidobacteria, may be contributing to brGDGT production in Rotsee

Supporting Information:

Supporting Information may be found in the online version of this article.

Correspondence to:

F. Ajallooeian,
fatemeh.ajallooeian@earth.ox.ac.uk

Citation:

Ajallooeian, F., Dubois, N., Ladd, S. N., Lever, M. A., Schubert, C. J., & De Jonge, C. (2025). Controls on brGDGT production in the seasonally anoxic water column and sediments of rotsee (Lake Rot). *Journal of Geophysical Research: Biogeosciences*, *130*, e2025JG009132. https://doi.org/10.1029/2025JG009132

Received 27 MAY 2025
Accepted 18 NOV 2025

Author Contributions:

Conceptualization: Fatemeh Ajallooeian, Nathalie Dubois, S. Nemiah Ladd, Mark Alexander Lever, Carsten Johnny Schubert, Cindy De Jonge
Data curation: Fatemeh Ajallooeian
Formal analysis: Fatemeh Ajallooeian
Funding acquisition: Cindy De Jonge
Investigation: Fatemeh Ajallooeian, Cindy De Jonge
Methodology: Fatemeh Ajallooeian, Mark Alexander Lever, Cindy De Jonge
Project administration: Nathalie Dubois, Carsten Johnny Schubert, Cindy De Jonge
Resources: Carsten Johnny Schubert, Cindy De Jonge

Abstract Reliable paleotemperature proxies are essential for reconstructing past climate. To refine interpretation of the MBT'_{5ME} index, based on bacterial brGDGT lipids, a year-long study was conducted in Rotsee, Switzerland, a seasonally stratified lake with a 4–21°C temperature range. Suspended particulate matter was collected monthly from the epilimnion and the hypolimnion, complemented by surface sediments and surrounding soils. Both intact polar (IPL) and core lipid (CL) brGDGTs were analyzed alongside 16S rRNA gene data to disentangle environmental (temperature, dissolved oxygen, and pH) and biological (microbial community) controls on brGDGT compositions. In the stratified epilimnion, MBT'_{5ME} values showed a muted response to summer warming ($r = 0.59$, $p < 0.1$), whereas the isomer ratio (IR) correlated more strongly with temperature ($r = 0.68$, $p < 0.05$). MBT'_{5ME} and IR were also significantly correlated ($r = 0.93$, $p < 0.0001$), providing a novel diagnostic tool to identify sedimentary GDGTs derived from surface waters. In the seasonally anoxic hypolimnion, MBT'_{5ME} correlated with pH ($r = 0.79$, $p < 0.01$) and IR with dissolved oxygen ($r = -0.65$ and $p < 0.05$). Microbial DNA analysis revealed low Acidobacterial abundances (<0.4% of reads), suggesting MBT'_{5ME} patterns are not solely driven by this phylum. Instead, hypolimnion IPL-brGDGTs correlated with gene abundance of several other bacteria, indicating broader microbial contributions. Surface sediments reflected an integrated water column signal, while also showing evidence for additional in situ IPL-brGDGT production. Overall, findings demonstrate that stratification onset drives MBT'_{5ME} variability, while epilimnion temperature exerts stronger control on IR, refining their application in paleoclimate proxies.

Plain Language Summary Understanding past climate change relies on chemical "proxies" that record environmental conditions. One such proxy, the MBT'_{5ME} index, is based on special bacterial lipids (brGDGTs) preserved in lake sediments. However, the processes controlling these lipids are still debated. We studied Rotsee, a small Swiss lake that develops warm surface waters and cold, oxygen-poor bottom waters each summer. Over 1 year, we collected monthly water samples from both layers, along with sediments and nearby soils. We measured bacterial lipids and DNA and compared them with environmental factors such as temperature, oxygen, and pH. In surface waters, MBT'_{5ME} responded only weakly to summer warming, but another measure, the isomer ratio (IR), tracked temperature more clearly. The two indices were also strongly linked, suggesting IR can help identify lipids that truly reflect surface water signals. In deep waters, MBT'_{5ME} was instead influenced by pH, while IR reflected oxygen availability. DNA analysis showed that not only Acidobacteria but also several different bacterial groups potentially contribute to brGDGT production. Overall, our findings show that lake mixing and stratification shape these lipid signals. This can improve the reliability of brGDGTs as tools for reconstructing past climates from lake sediments.

1. Introduction

Understanding local climate variability is essential for interpreting both present and future climate change (Kaufman et al., 2020). Among available proxies, bacterial membrane lipid biomarker branched glycerol dialkyl glycerol tetraethers (brGDGTs) are widely applied in paleothermometry (Schouten et al., 2013). Empirical calibrations, based on the temperature dependency of brGDGT distributions on global and continental scales (Weijers et al., 2006), have enabled high-resolution temperature reconstructions in lake sediments across East

Supervision: Mark Alexander Lever, Cindy De Jonge
Visualization: Fatemeh Ajallooeian
Writing – original draft: Fatemeh Ajallooeian
Writing – review & editing: Fatemeh Ajallooeian, Nathalie Dubois, S. Nemiah Ladd, Mark Alexander Lever, Carsten Johnny Schubert, Cindy De Jonge

Africa (Loomis et al., 2012), North America (Watson et al., 2018), Asia (Wu et al., 2023; Zhu et al., 2021), South America (O'Beirne et al., 2025), and eastern Europe (Ramos-Roman et al., 2022). First identified in peatlands (Sinninghe Damsté et al., 2000), brGDGTs have since been found in soils (e.g., Weijers, Schouten, et al., 2007), lake sediments (e.g., Tierney & Russell, 2009), and suspended particulate matter (SPM) in freshwater systems (e.g., Russell et al., 2018; Zell et al., 2013). Variations in their degree of methylation form the basis of paleoclimate proxy MBT'$_{5ME}$, which correlates with air temperature in soils (Crampton-Flood et al., 2020; De Jonge et al., 2014; Peterse et al., 2012; Weijers, Schouten, et al., 2007) and lakes (Martínez-Sosa et al., 2021; Russell et al., 2018). The complementary isomer ratio (IR), which reflects the relative abundance of 6-methyl to 5-methyl brGDGTs, has been linked to variability in pH, water conductivity, and salinity (De Jonge et al., 2014; Raberg et al., 2021; Wang et al., 2021).

While global calibrations correlate MBT'$_{5ME}$ values with temperature in lakes, growing evidence shows that temperature alone does not explain the observed variability in brGDGT distributions (Martínez-Sosa et al., 2021; Russell et al., 2018). Factors such as dissolved oxygen (Colcord et al., 2017; Weber et al., 2018; Wu et al., 2021), mixing regimes and depth (Baxter et al., 2024; Crampton-Flood et al., 2020; Stefanescu et al., 2021; van Bree et al., 2020), nutrient availability (Hu et al., 2016), pH (Weijers, Schefuß, et al., 2007), and alkalinity (Schoon et al., 2013) can also influence brGDGT distributions. These environmental drivers not only impact brGDGT concentrations (Ajallooeian et al., 2024b; Loomis, Russell, Eggermont, et al., 2014) but also alter MBT'$_{5ME}$ and IR, complicating their interpretation in paleoclimate reconstructions.

To fully understand the impact of environmental factors on brGDGT variation, the mechanisms underlying brGDGT variability must be identified. MBT'$_{5ME}$ values are thought to reflect homeoviscous adaptation to temperature within the bacterial phylum Acidobacteria, a physiological response supported by membrane modeling approaches (Naafs et al., 2021) and confirmed through temperature-dependent brGDGT production in pure culture experiments (Chen et al., 2022; Halamka et al., 2022). However, not all brGDGTs found in nature are produced by Acidobacteria. While early environmental studies identified Acidobacteria as dominant brGDGT producers in soils (De Jonge et al., 2019; Halffman et al., 2022; Peterse et al., 2010; Weijers et al., 2009), biosynthetic genes for synthesis of membrane-spanning ether lipids were recently detected across a wide range of bacterial taxa, including not only Acidobacteria but also Proteobacteria and Firmicutes (Sahonero-Canavesi et al., 2022; Zeng et al., 2022). While Acidobacteria can be abundant in lake sediments (Rodriguez et al., 2025), yet their low abundances in lake water columns (Berg et al., 2022; Dedysh & Sinninghe Damsté, 2018; Han et al., 2020) suggest a broader range of brGDGT producers in these environments (Weber et al., 2018). Environmental studies indicate that changes in the microbial community across oxygen and pH gradients can drive changes in brGDGT distributions (De Jonge et al., 2019, 2021; Weber et al., 2018). 16S rRNA gene sequencing allows specific bacterial taxa to be correlated with brGDGT compound concentrations, helping constrain which organisms potentially produce these biomarkers in natural systems. Thus, correlating bacterial community composition with specific brGDGT compounds provides indications of potential producers.

In contrast to soils, where brGDGTs have a long turnover time (Weijers et al., 2010) and stable distributions across seasons (Naafs et al., 2017; Weijers et al., 2011), lake water columns exhibit significant seasonal variability in brGDGT concentrations and distributions (Loomis, Russell, Heureux, et al., 2014; Miller et al., 2018; van Bree et al., 2020). Consequently, the depth and production season of brGDGTs within the lake water column can affect the temperature signal. If brGDGTs are predominantly produced in the deeper (hypolimnion) water layer (Bechtel et al., 2010; Buckles et al., 2014; Weber et al., 2018), the record may exclude summer warming that mainly impacts surface (epilimnion) waters. Conversely, seasonal production in the epilimnion could reflect spring, summer, or autumn temperatures rather than annual averages (Loomis, Russell, Heureux, et al., 2014; Miller et al., 2018). Contributions of brGDGTs from soils (Peterse et al., 2009; Weber et al., 2018) can also complicate sedimentary records, highlighting the need to constrain their provenance for accurate paleoclimate reconstruction.

Although previous studies on brGDGTs in lake systems have identified that seasonality and water column stratification affect brGDGT distributions, fundamental questions about production mechanisms remain. Previously, temporal studies analyzed only core lipids (Loomis, Russell, Heureux, et al., 2014), while studies examining both intact polar lipids (IPLs) and core lipids (CL) had limited temporal resolution (Buckles et al., 2014) or focused on permanently stratified systems where environmental gradients remain confounded (Baxter et al., 2024). Crucially, none combined high-resolution seasonal sampling with simultaneous IPL and CL analysis and microbial community identification.

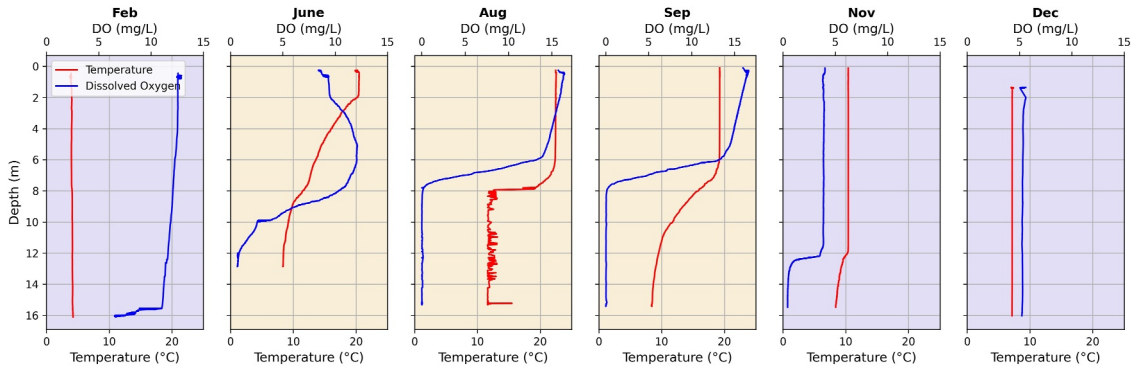

Figure 1. Vertical profiles of temperature (°C, red) and dissolved oxygen (mg L^{-1} blue) in the water column of Rotsee during selected months. Isothermal mixing periods (February, November, and December) are shown in blue shading, and stratified periods (June, August, and September) are shown in orange shading.

To address these methodological gaps, we paired high-resolution seasonal sampling with both intact polar lipid (IPL) and core lipid analysis with microbial community identification in Rotsee, a small lake in central Switzerland. It provides an ideal natural laboratory as its seasonal stratification from May to October creates distinct oxic (epilimnion) and seasonally anoxic (hypolimnion) zones (Naeher et al., 2014) and thus naturally separates the effects of temperature and redox conditions. Previous laboratory mesocosm experiments at this location showed muted MBT'_{5ME} temperature responses, providing a useful frame of reference for investigating natural seasonal dynamics across the 17°C temperature range. Here, we use data from Rotsee to address three key questions: (a) how do temperature, pH, and oxygen control brGDGT distributions in different lake zones; (b) when and where are different brGDGTs actively produced, as revealed by IPL versus core lipid distribution; and (c) what is the role of seasonal changes in microbial community structure in driving brGDGT compositions?

2. Materials and Methods

2.1. Water Column, Surface Sediment, and Soil Sampling

Rotsee (47°21′05.8″ N; 8°31′12.7″ E) is a small, eutrophic, subalpine lake with a surface area of 0.48 km^2 and a maximum depth of 16 m (Naeher et al., 2014). Rotsee does not freeze during winter, with surface water temperatures remaining above 0°C year-round (Figure 1). The lake is monomictic, undergoing annual thermal stratification during the warm season. Stratification leads to hypolimnion anoxia due to high aerobic mineralization rates of phytoplankton-derived organic matter (Naeher et al., 2014; Schubert et al., 2010).

Water samples were selected from a series of sampling dates that occurred every two to four weeks at Rotsee between February and December 2019. Samples were taken from two depths: 0–1 m (epilimnion) and 14–15 m (hypolimnion, 1 m above the sediment surface) using a 20 L Niskin sampler. Ten timepoints were chosen for analysis. At each timepoint, temperature, conductivity, pH, and dissolved oxygen were measured using a CTD scanner (Sea and Sun Technology®, Germany). Mean annual air temperature (MAAT) was determined by averaging monthly air temperature data for the sampling period. Monthly temperatures were obtained from Federal Office of Meteorology and Climatology MeteoSwiss (2019). Water alkalinity was determined from aliquots collected at both depths using a Compact Titrosampler (Metrohm Inc., Switzerland). Approximately 40 L of lake water from each layer was temporarily stored at 4 °C and filtered within 12–24 hr of sampling. Suspended particulate matter (SPM) was collected in 0.7-µm GF/F filters (Durapore®, Germany) using a titanium tripod cleaned with EtOH and MilliQ water between samples. Filtered water underwent a second filtration step with 0.22 µm PVDF (polyvinylidene fluoride) filters (Durapore®, Germany) to capture smaller particles and free-living bacteria. For select timepoints (17.07.2019, 14.08.2019, and 18.12.2019), aluminum sulfate was added to prefiltered water to coagulate dissolved organic matter (DOM), which was subsequently collected on the 0.7 µm filters. This method effectively flocculates DOM (Masion et al., 2000). Filters were wrapped in aluminum foil and stored at −20°C.

To investigate the provenance of sedimentary brGDGTs, the data set included four surface sediment samples collected along a depth transect (0–4 cm sediment depth) in April 2024. These samples were taken from depths of 0.5 m (S0.5, $n = 2$) and 5.5 m (S6, $n = 1$) (both located above the seasonal oxycline) and at 11 m (S11, $n = 1$), which was below the seasonal oxycline. Additionally, five soil samples from the surrounding watershed (0–5 cm

depth) were collected, including anthropogenic wetland, grassland, and forest (Table S1). While sediment pore water oxygen was not measured, depletion within the top 0.5 cm is expected.

2.2. Lipid Extraction

To distinguish between recently produced brGDGTs and their more stable, preserved counterparts, both intact polar lipids (IPLs) and core lipids (CL) brGDGTs were measured and analyzed.

From the 0.7 μm filter samples, a fraction of the filter ($n = 20$) was collected for DNA extraction (~16 mm^2 per filter), while the remaining material was freeze-dried. Additional PVDF ($n = 6$), DOM ($n = 2$), surface sediment ($n = 4$), and soil samples ($n = 5$) were also freeze-dried for lipid extraction. Filters were divided into three sections: (E1) underwent lipid extraction using a modified Bligh-Dyer method (BDE + TCA) with a solvent mixture of methanol (MeOH), dichloromethane (DCM), and phosphate buffer (2:1:0.8, v/v/v) for three rounds of ultrasonic extraction, followed by three additional rounds with 5% trichloroacetic acid (TCA) substituted for phosphate buffer. DCM was added to each extraction step, and the combined DCM phases constituted the total lipid extract (TLE) (Sturt et al., 2004; modified from Pitcher et al., 2009; Huguet et al., 2010). (E2) underwent acid hydrolysis (AH) directly on the filter material, using 1.5 N HCl in MeOH (v/v) at 80°C for 2 hr to convert IPLs to CLs after Weber et al. (2017). The third section (E3) was archived. Surface sediment samples were similarly extracted using the modified BDE + TCA and acid hydrolysis methods. Soil brGDGTs were extracted using an automated EDGE solvent extraction system (EDGE, ©CEM Corporations, USA, after De Jonge et al. (2024)) with DCM/MeOH (1:1, v/v) as the solvent, 3x, generating a fraction dominated by CL brGDGTs, with an unknown contribution of IPL brGDGTs.

The TLEs from SPM, sediment, and soil samples were separated into fractions of different polarities using a Pasteur pipette column packed with 3.5 cm of activated aluminum oxide. Nonpolar, ketone, and polar fractions were collected using hexane/DCM (9:1, v/v), hexane/DCM (1:1, v/v), and DCM/MeOH (1:1, v/v), respectively. Before analysis, 49.6 ng of a GTGT internal standard (C46) was added to the polar fraction (following Huguet et al., 2006), which was subsequently filtered through a 0.45-μm PTFE filter, dried under N_2, and redissolved in 50 μL of hexane/isopropanol (99:1, v/v). Samples were analyzed on a high-performance liquid chromatography-mass spectrometry (HPLC–MS; Agilent Technologies®-1200) following Hopmans et al. (2016), using a modified column temperature of 40°C and a 10-μL injection volume.

Instrument error for semiquantification of brGDGT concentrations was estimated at 15%–20% based on duplicate analysis of 6 SPM samples (0.7 μm filters). IPL brGDGT quantities were calculated by subtracting concentrations of CL brGDGTs (E1) from total brGDGTs (E2), with propagated errors of 17%–21%. IPL compounds with negative concentration values were assigned a value of zero.

The following formulas and calibrations were applied in this study:

$$MBT'_{5ME} = \frac{Ia + Ib + Ic}{Ia + Ib + Ic + IIa + IIb + IIc + IIIa}$$ (De Jonge et al., 2014)

$$IR = \frac{IIa' + IIIa'}{IIa' + IIIa' + IIa + IIIa}$$ (De Jonge et al., 2021)

Mean Annual Temperature (MAT) $= -1.21 + 32.42 \times MBT'_{5ME}$ ($r2 = 0.92, p < 0.0001, RMSE = 2.44$ °C (Russell et al., 2018).

2.3. Quantification and Sequencing of 16S rRNA Genes

To assess bacterial variability, DNA extraction followed the modular protocol of Lever et al. (2015). To minimize DNA adsorption, a 10-mM dNTP solution was added, followed by cell lysis with a chemical treatment using a shaker at 50°C for 1 hr. The DNA-containing supernatant was separated via centrifugation (10 min, 14,000 × g), washed twice with cold chloroform-isoamyl alcohol (24:1), and precipitated using NaCl, linear polyacrylamide (LPA; 20 μg mL^{-1} extract), and ethanol (EtOH) at room temperature in the dark for 2 hr. DNA pellets were obtained through centrifugation (20 min, 14,000 × g), washed thrice with 70% EtOH, dried, and dissolved in molecular biology-grade water (H_2O). Negative controls, including molecular-grade H_2O and extraction blanks, confirmed minimal contamination, with 16S rRNA gene copy numbers over 1,000-fold lower than those in Rotsee DNA extracts. qPCR standards were based on dilution series (10^1–10^7) of full-length 16S rRNA gene plasmids from Rhodobacter sphaeroides.

From 18 successfully amplified samples, a 16S rRNA gene amplicon sequence library was prepared following Deng et al. (2020). Amplicons were generated using primer pairs S-D-Bact-0341-b-S-17 (5′-CCTACGGGNGG CWGCAG-3′) and S-D-Bact-0785-a-A-21 (5′-GACTACHVGGGTATCTAATCC-3′) and sequenced on an Illumina MiSeq platform. Positive controls (16S rRNA plasmids from *Holophaga foetida*) and contamination controls (H_2O and extraction blanks) were included to ensure data quality.

Minimal data loss (<5%) occurred during raw sequencing back-mapping, resulting in 14,608 zero-radius operational taxonomic units (zOTUs). After singleton exclusion, 7,545,540 amplicon reads corresponding to 8,501 zOTUs were retained for analysis. Reads were clustered into OTUs at a 97% identity threshold, with phylogenetic assignments performed using the SILVA database (https://www.arb-silva.de/; Deng et al., 2020).

For decontamination, a combined approach using both frequency-based contaminant identification and known contaminant filtering was employed. Frequency-based decontamination was performed using the "decontam" R package (Davis et al., 2018), which identifies contaminants based on their inverse correlation with sample DNA concentration (16S rRNA gene copies per ml). Additionally, we filtered known contaminant genera commonly identified in laboratory reagents and kits based on previously published studies (Salter et al., 2014; Sheik et al., 2018), including Pseudomonas, Propionibacterium, Ralstonia, and Acinetobacter, among others.

Following these steps, we further refined our decontamination approach by conducting BLAST (basic local alignment search tool) searches in NCBI (National Center for Biotechnology Information) database for remaining OTUs and filtered out families that matched known human skin, gut microbiota, or pathogens. We assessed the top 10 closest BLAST hits for each sequence, with highly likely contaminants showing very high sequence similarities (>99%) to either pure culture strains isolated from human environments or "environmental sequences" from human environments. Suspicious sequences also included those reported from laboratory reagents, the human microbiome, and ultralow biomass environments (e.g., air, glacial ice, and groundwater). This additional screening resulted in the removal of three more families: Carnobacteriaceae, Alcaligenaceae, and Microbacteraceae. Finally, the sequence reads were rarified to a sample depth of 234,884 reads per sample, reducing the data set to 6,590 OTUs across 16 samples for further analysis, minimizing sequencing depth biases.

To investigate potential microbial associations, Spearman correlations were calculated between the top 95% most abundant orders and brGDGT concentrations. OTU-relative abundances were transformed to concentrations by multiplying the relative abundance of each OTU with the mean gene concentration of each sample (averaged from three qPCR replicates).

2.4. Statistical Methods

The mean ($\bar{x}$) and standard deviation (σ) values of brGDGT fractional abundances, ratios for core lipids (CL), and intact polar lipids (IPL) were calculated to assess variability over time in the epilimnion and the hypolimnion. Since two compounds (brGDGT IIIc and IIIc') were consistently below the detection limit, calculations were based on 13 brGDGTs. Yearly weighted averages (WA) for brGDGT fractional abundances and ratios were calculated by applying linear weights based on normalized monthly concentrations, with higher weights assigned to months with greater concentrations. For this calculation, the average values for March and May were used to estimate the missing value for the month of April.

To explore environmental drivers of brGDGT variability, Pearson correlation coefficients (r) were computed using the "scipy.stats" package (Python v.3.8.5). Principal component analysis (PCA) was performed on standardized fractional abundances using "vegan" (Oksanen et al., 2013) in R (v.4.2.3). A stepwise forward selection analysis (Dray et al., 2006; Legendre & Legendre, 2012) was also implemented in "vegan", following the variance-partitioning framework (Blanchet et al., 2008). The procedure begins with the parameter explaining the most variance, tests its significance using 499 Monte Carlo permutation tests, and sequentially adds further variables only if they significantly increase the explained residual variance. The process stops when additional variables no longer explain residual variance.

Environmental and microbiome data were analyzed in R (v4.1.2) using the "phyloseq", "vegan," and "indicspecies" packages (De Cáceres, 2013; McMurdie & Holmes, 2013; Oksanen et al., 2013). Bacterial communities were aggregated at the order level, retaining the top 95% most abundant orders ($n = 57$) for analysis. Indicator species analysis was performed to identify OTUs characteristic of the epilimnion or the hypolimnion, using 999 permutations with a corrected significance threshold ($p < 0.05$). Spearman correlation analyses explored

relationships between bacterial community composition and environmental parameters. In the epilimnion, correlations were examined between bacterial orders' relative abundance and temperature. In the hypolimnion, dissolved oxygen relationships were instead assessed. Additionally, correlations were analyzed between bacterial orders' absolute abundance and concentrations of five specific brGDGT compounds (Ia, IIa, IIIa, IIa', and IIIa'). Data handling and visualization were performed using "tidyverse", "pheatmap", and "ggplot2" (R), and matplotlib, seaborn, and ternary (Python v3.8.5), respectively.

3. Results

3.1. Mixing Regime and Water Chemistry

In 2019, thermal stratification in Rotsee began in mid-May, with the thermocline and oxycline stabilizing at a depth of 6–7 m during July and August (Figure 1). As the epilimnion cooled in autumn, water column mixing deepened the stratified layer from September to November, resulting in a fully mixed water column by December (Figure 1). Epilimnion temperatures varied substantially throughout the year (4–21°C), with February and August being the coldest and warmest months, respectively. In contrast, the hypolimnion exhibited more limited temperature variation (4–9°C) but also reached its highest temperature in August (Figure 2a).

Seasonal mixing and thermocline development impacted dissolved oxygen (DO) concentrations (Figure 1). During the winter-spring mixing period, DO levels were stable in both the epilimnion and the hypolimnion, averaging around 11 mg L^{-1}. As stratification progressed, epilimnion oxygen concentrations increased, peaking at 15 mg L^{-1}. Conversely, hypolimnion DO levels decreased from May onward, dropping below 2 mg L^{-1} by June (suboxic conditions) and reaching anoxic levels (<0.1 mg L^{-1}) from August to October (Figure 2e). During autumn mixing, oxygenated water from the epilimnion reached the hypolimnion, restoring uniform oxygen concentrations by December.

Seasonal stratification affected additional water chemistry parameters. In the epilimnion, conductivity correlated strongly with temperature ($r = 0.66$, $p < 0.05$). In the hypolimnion, conductivity and alkalinity were negatively correlated with dissolved oxygen ($r = -0.89$ and -0.60, respectively; $p < 0.05$). Hypolimnion alkalinity increased with the onset of anoxic conditions during stratification, while epilimnion alkalinity decreased during this period (Figure 2c).

Water pH displayed oscillations independent of stratification (Figure 2d). In the epilimnion, pH remained stable during spring mixing and stratification ($\bar{x} = 8.1$, $\sigma = 0.1$) but dropped to 7.1 during autumn mixing (Figure 2d). In the hypolimnion, pH decreased (<7.1) during stratification but increased to 8.8 with the onset of isothermal mixing (Figure 1).

3.2. Patterns of brGDGTs' Suspended Particulate Matter (SPM)

3.2.1. BrGDGT Concentration Variability

The 0.22 μm (PVDF filters) and DOM samples yielded significantly lower summed brGDGT concentrations (1–11 ng L^{-1}) than the 0.7-μm filters and often included only brGDGT Ia, IIa, and IIIa (Table S1). Since 0.7 μm fraction captured 95% of brGDGTs in the SPM, the discussion is therefore limited to 0.7 filters (Table S1). Summed concentrations of CL brGDGTs varied with depth and season (Table S1; Figure 3a). Throughout the year, IPL brGDGTs constituted ~15% of the total brGDGT pool in the epilimnion and ~20% in the hypolimnion.

In the epilimnion, CL brGDGT Ia was the most abundant compound, reaching a maximum concentration of 0.85 ng L^{-1} in July. Elevated levels persisted until August before declining to 0.22 ng L^{-1} in December (Figure 3b). BrGDGT IIa showed stable concentrations throughout the year and was positively correlated with Ia ($r = 0.67$ and $p < 0.05$). BrGDGT IIIa had lower concentrations, averaging 0.47 ng L^{-1} until September, after which it increased to 0.70 ng L^{-1} during October to December (Figure 3c). Despite opposite seasonal trends between Ia and IIIa (Figure S1A in Supporting Information S1), no significant negative correlation was observed. When averaged over the whole year, the 6-methyl brGDGTs were more abundant than their 5-methyl counterparts in the epilimnion (Figure 3b). BrGDGT IIa' exhibited a similar seasonal pattern to Ia, with concentrations peaking at 0.94 ng L^{-1} in July and decreasing to 0.26 ng L^{-1} in December. BrGDGT IIIa' peaked in July (1.17 ng L^{-1}), maintained high concentrations through summer, and declined to 0.37 ng L^{-1} in December (Figure 3b).

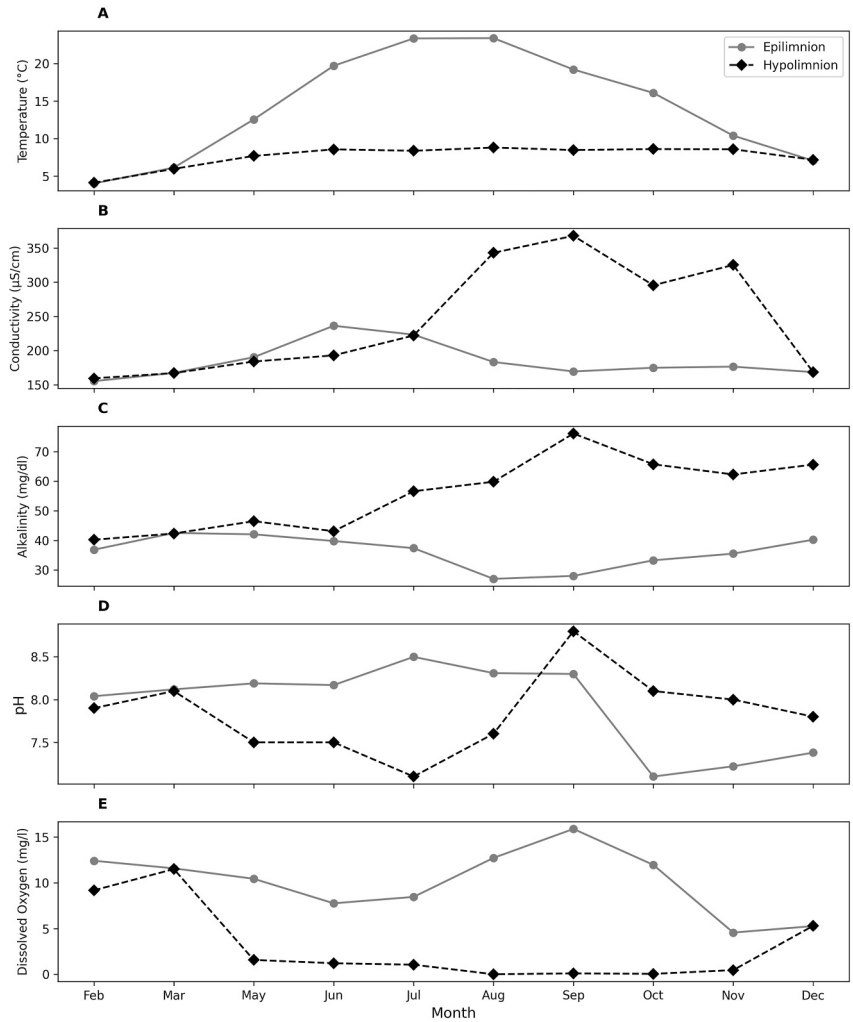

Figure 2. The variability of inorganic parameters for the epilimnion and the hypolimnion of Rotsee, with time specifically, (a) temperature (°C), (b) conductivity (µS cm^{-1}), (c) alkalinity (mg dl^{-1}), (d) pH, and (e) dissolved oxygen (DO; mg L^{-1}).

In the seasonally anoxic hypolimnion, brGDGT IIIa was the dominant compound, ranging from 0.1 to 2.1 ng L^{-1} (Figure 3c). Unlike in the epilimnion, IIIa strongly correlated with Ia ($r = 0.93$ and $p < 0.01$) and IIa ($r = 0.98$ and $p < 0.01$) (Figure S1A in Supporting Information S1). The 6-methyl isomers (IIa' and IIIa') were less abundant in the hypolimnion than in the epilimnion, but IIIa' was still a prominent compound, averaging 0.8 ng L^{-1} ($\sigma = 0.5$ ng L^{-1}) (Figure 3c).

IPL brGDGTs compounds Ia, IIa, IIIa, IIa', and IIIa' were detected only periodically, in June, August, October, and November in the epilimnion and February, August, and September in the hypolimnion (Figures 3d and 3e). Hypolimnion IPL brGDGT concentrations peaked in August at 3.62 ng L^{-1}. In contrast with the CL distributions, IPL brGDGT Ia was not the most abundant compound in either the epilimnion (4%–12%) or the hypolimnion (3%–15%) (Table S1). In the epilimnion, 6-methyl brGDGTs constituted the largest fraction of IPLs (21%–29%), while in the hypolimnion, IPL brGDGT IIIa was the most abundant (~38%) (Figures 3d and 3e; Table S1).

3.2.2. BrGDGT Distribution Variability

The seasonal changes in the concentrations of CL brGDGTs in the epilimnion and the hypolimnion of Rotsee result in distributional changes that are summarized as variations in brGDGT ratios MBT'_{5ME} and IR. In the epilimnion, MBT'_{5ME} varied between 0.22 and 0.53, with a weighted average value of 0.39 (Figure 4a). The

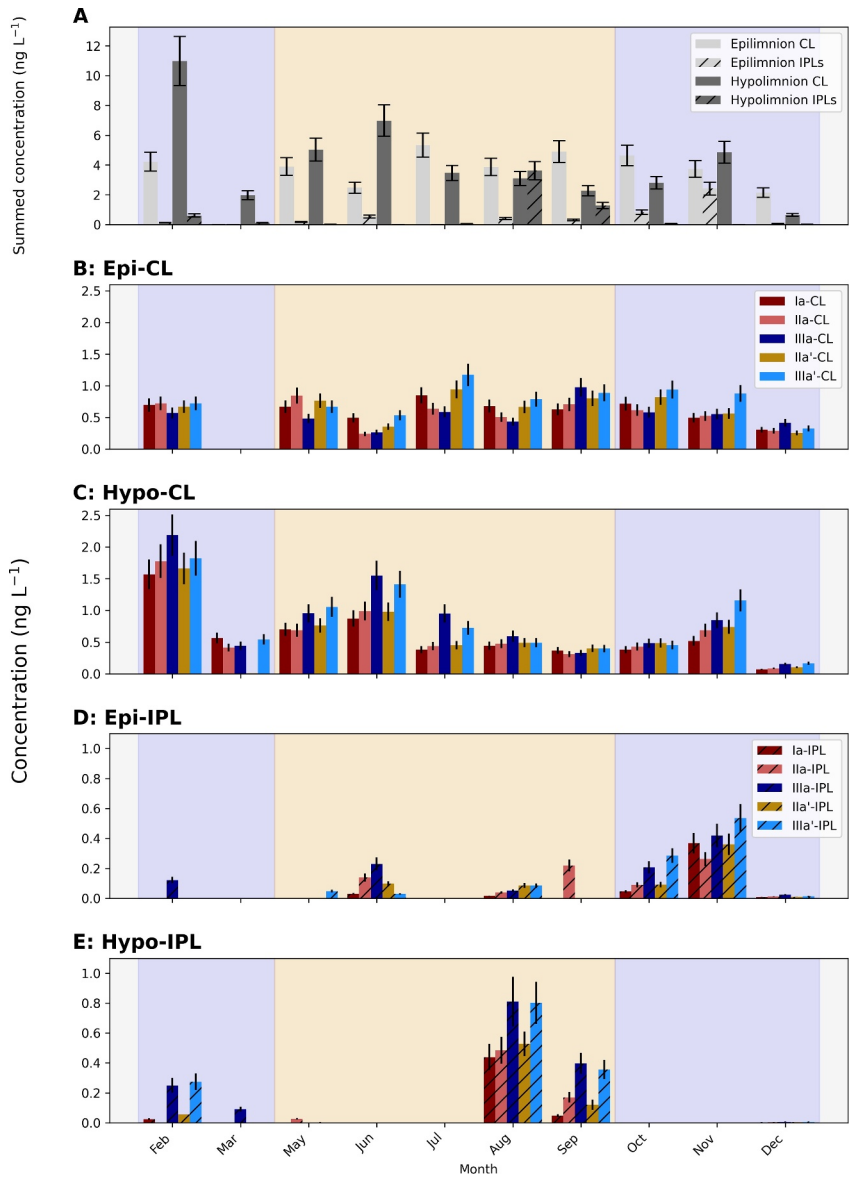

Figure 3. Seasonal variability of brGDGT concentrations in Rotsee. (a) Summed concentrations of brGDGTs (ng L^{-1}) in the epilimnion (light gray) and the hypolimnion (dark gray). (b)–(e) Concentrations of the five most abundant individual brGDGTs, shown separately for epilimnion and hypolimnion core lipids (CL; panels (b) and (c)) and intact polar lipids (IPL; panels (d) and (e)). Error bars indicate 15% instrumental error, propagated for the calculated IPL concentrations. Background shading highlights Rotsee seasonal water column dynamics: blue areas (samples 1–2 and 8–10) represent isothermal mixing periods (winter, early spring, late fall), while orange (samples 3–7) indicates stratification (late spring, summer, and early fall).

variation in MBT'_{5ME} generally exhibited small changes from February to May (0.38–0.39), caused by a stable fractional abundance of the major brGDGTs Ia, IIa and IIIa (Figure 4c).

In June, the CL MBT'_{5ME} showed a significant increase, attributed to the high fractional abundance of brGDGTs Ia (20%) and Ib (8%) (Table S1), which continued until August. In September, a drop in MBT'_{5ME} value (0.31) was coeval with an increased fractional abundance of brGDGTs IIb (>6%) and IIIa (20%), while in December, MBT'_{5ME} also declined (0.22), caused by a lower fractional abundance of brGDGTs Ia (<15%) and Ib (<4%), along with an increased fractional abundance of IIIa (>30%) (Table S1). MBT'_{5ME} values were converted to reconstructed temperature (T_{rec}) using the global lacustrine calibration of Russell et al. (2018) (Figure 4). In the epilimnion, measured water temperatures and GDGT-derived T_{rec} showed a weak positive correlation ($r = 0.59$

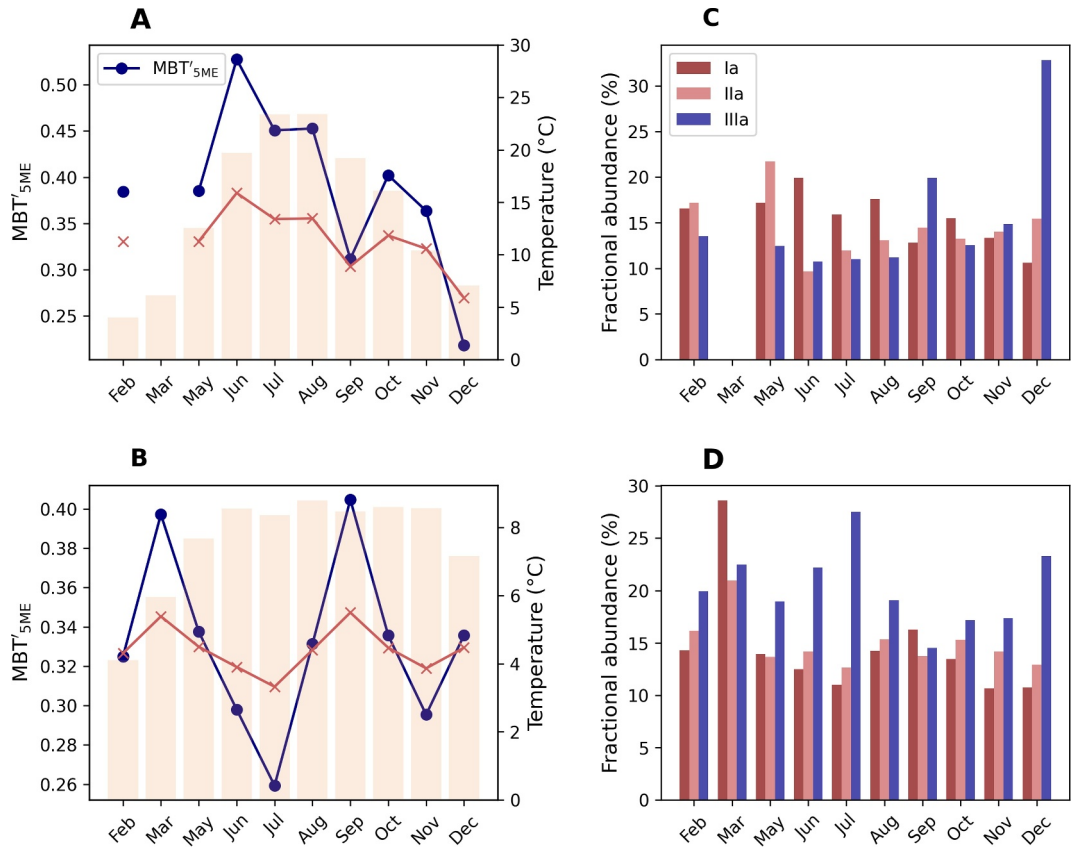

Figure 4. Comparing brGDGT-based ratio MBT'$_{5ME}$ values (dark blue) and the MBT'$_{5ME}$-based reconstructed temperature (T_{rec}, red), with measured water temperature at the depth of sampling (shaded orange bars). The fractional abundance of brGDGTs Ia, IIa, and IIIa is plotted in panels (c) and (d). Panels (a) and (c) depict epilimnion values; panels (b), (d) depict hypolimnion.

and $p = 0.09$). In addition, MBT'$_{5ME}$ and IR were strongly correlated in the epilimnion ($r = 0.93$ and $p < 0.0001$; Figure 5 and Figure S2 in Supporting Information S1).

In the hypolimnion, the range of MBT'$_{5ME}$ values (0.25–0.40) was narrower than the epilimnion (Figure 4b). MBT'$_{5ME}$ showed maxima in March and September and decreased in June–July and November–December (Figure 4b), while in March, a high fractional abundance in Ia was responsible for the elevated MBT'$_{5ME}$; in September, the decreased fractional abundance of IIIa along with a relative increase in Ib accounted for the increase in MBT'$_{5ME}$ value (Figure 4d, Table S1). In July, the low fractional abundance of brGDGT Ia and high fractional abundance of IIIa drive the minimum MBT'$_{5ME}$ value (<0.25). No significant correlation between T_{rec} and measured temperature was observed in the hypolimnion ($r = -0.20$, $p = 0.58$).

Reflecting the constant relative abundance of 5 and 6-methyl brGDGTs (Table S1), the epilimnion showed low variability in IR values ($\bar{x} = 0.56$, $\sigma = 0.06$; Figure 5a).

In the hypolimnion (Figure 5b), IR values were similar to those observed in the epilimnion. March stands out with a noticeably low IR value (0.38) caused by a low (<2%) fractional abundance of IIa'. In July and September, variability in the IR values was caused by changes in the fractional abundance of IIIa.

3.3. Rotsee 16S rRNA Gene-Based Bacterial Community

The qPCR-derived 16S rRNA gene copy numbers (counts mL^{-1}) in seasonal SPM fluctuated throughout the year, with increases and decreases corresponding to stratified and mixing periods, respectively, in both the epilimnion and the hypolimnion (Figure 6a). The composition of the 16S rRNA gene-based bacterial community also exhibited seasonal variation (Figures 6a and 6b).

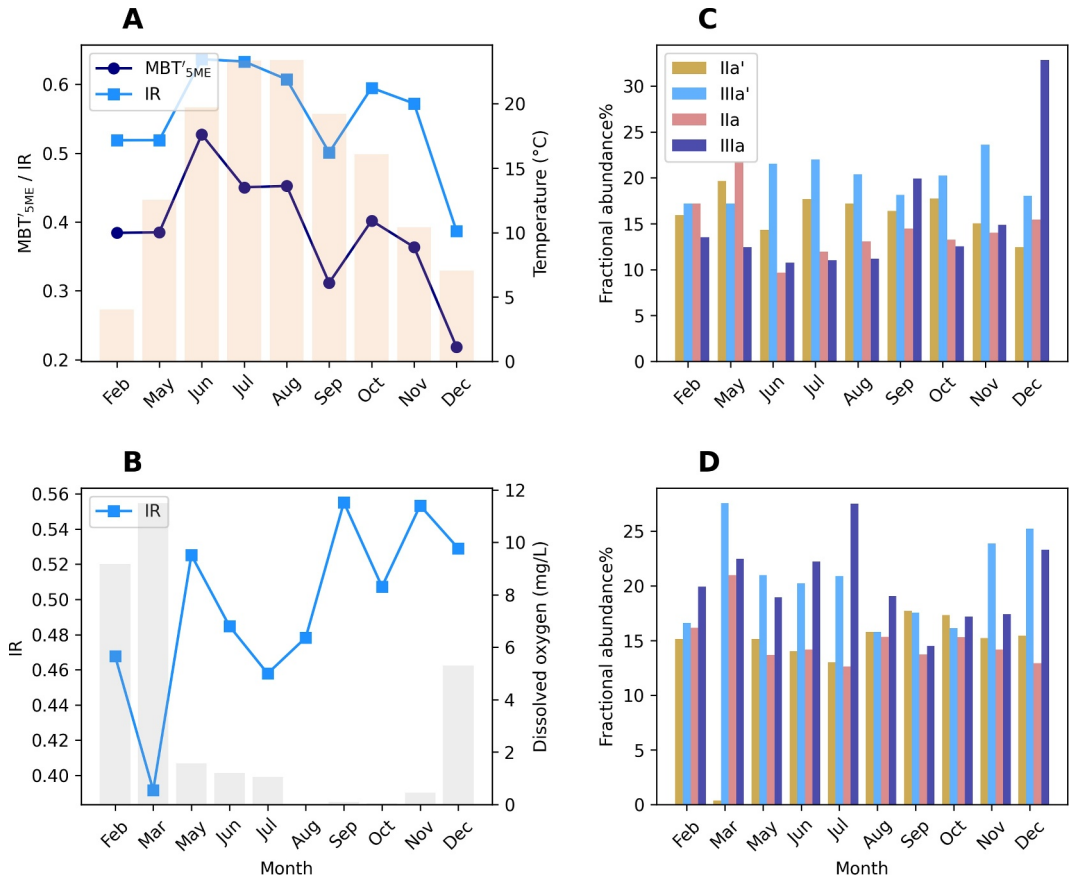

Figure 5. Plotting brGDGT isomer ratio (IR) values (light blue) and MBT'$_{5ME}$ values (dark blue) with measured epilimnion temperature (shaded orange bars) and dissolved oxygen plotted in (shaded gray bars). The fractional abundance of brGDGTs IIa, IIIa, IIa', and IIIa' is plotted in panels (c) and (d) Panels (a), (c), (b), and (d) depict epilimnion and hypolimnion values, respectively.

During periods of isothermal mixing, the bacterial community composition became more similar between the epilimnion and the hypolimnion, whereas the most pronounced differences between the epilimnion and the hypolimnion were observed during summer stratification (Figure 6b).

To identify which bacterial orders are characteristic of the epilimnion versus the hypolimnion, we determined bioindicator species by calculating z values that measure how strongly each order's abundance correlates with temperature in the epilimnion and with oxygen levels in the hypolimnion (Figure 6c).

3.4. BrGDGTs of Surface Sediments and Surrounding Soils

In the surface sediments, summed CL brGDGT concentrations are similar in shallow sediments (0.5 and 6 m depths), ranging from 159 to 203 ng g^{-1} sed but increase fivefold at the deepest site (Table S1). Variations in the fractional abundance of key brGDGTs, such as IIIa and IIIa', influence shifts in the MBT'$_{5ME}$ and IR indices (Table S1, Figures 4 and 5). The shallow sediments had a higher MBT'$_{5ME}$ value (0.40) than the intermediate sediment (0.26). At the deepest site, 5-methyl brGDGT Ia dominates (17%), yielding the warmest MBT'$_{5ME}$ value (0.43, T_{rec} = 12.7°C).

IPL brGDGT concentrations were lower but followed a similar depth pattern, peaking at 98.36 ng g^{-1} sed at the deepest site. In the soils surrounding Rotsee, summed CL brGDGT concentrations ranged from 202.4 to 2894.6 ng g^{-1} sed (Table S1). The distributions were dominated by 5-methyl brGDGT Ia ($\bar{x}$ = 25%, σ = 11%), yielding MBT'$_{5ME}$ values between 0.46 and 0.54 (T_{rec} = 13–16°C). IR values were consistently lower than those in lake surface sediments, ranging from 0.17 to 0.21.

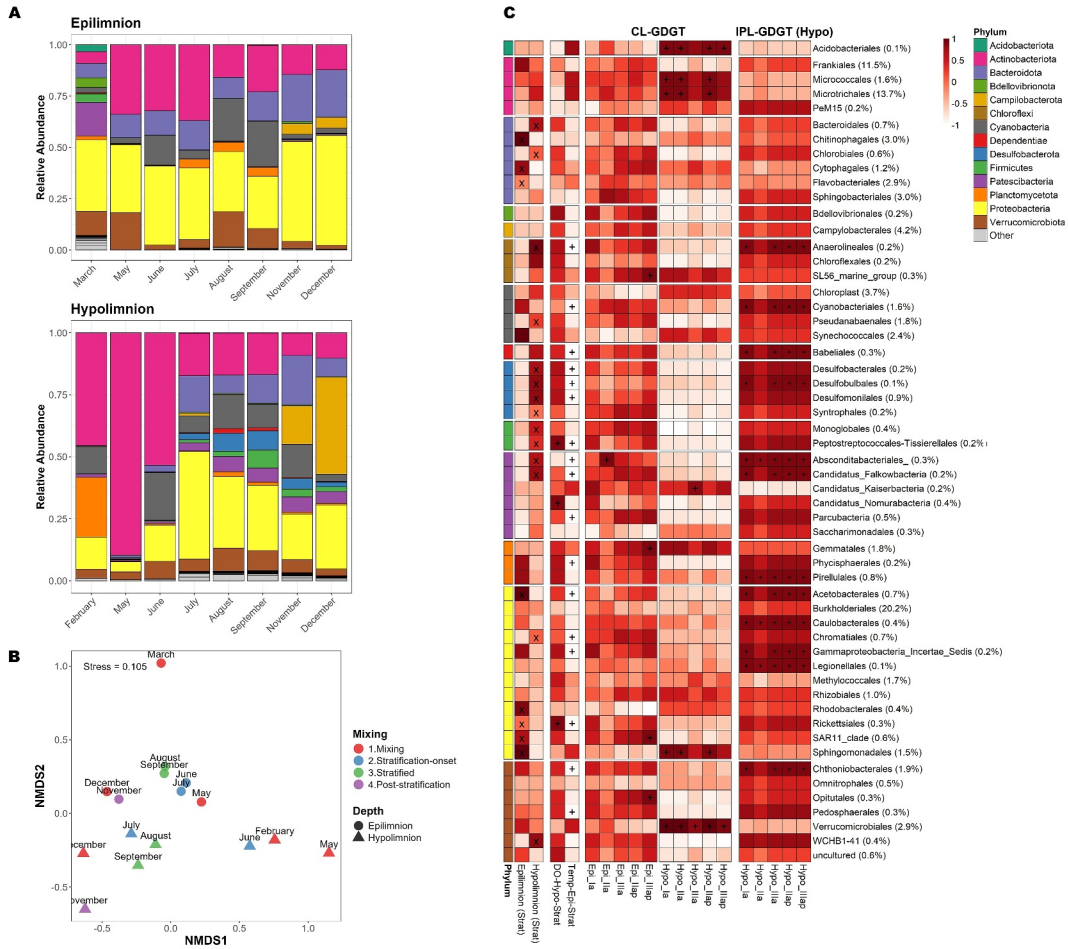

Figure 6. (a) Stacked bar charts showing relative abundance (0–1) of the top 95% most abundant bacterial phyla in the epilimnion and the hypolimnion of Rotsee across different months. Different colors represent distinct phyla as indicated in the legend. (b) Nonmetric multidimensional scaling (NMDS) of Rotsee bacterial community composition based on OTUs of the top 95% most abundant orders. Sample colors reflect water column mixing conditions, with shapes representing sampling depth: epilimnion (sphere) or hypolimnion (triangle). (c) Multipanel heat map of environmental and brGDGT dependency of bacterial orders, grouped per phylum (phyla are color-coded). From left to right: (1) Z scores showing relative abundance of each order during stratification in both the epilimnion and the hypolimnion. (2) Spearman correlation r values between bacterial orders and temperature in the epilimnion and dissolved oxygen in the hypolimnion during stratification. (3) Spearman correlation r values between bacterial orders and core lipid (CL) brGDGTs in both water column layers. (4) Spearman correlation r values between bacterial orders and intact polar lipid (IPL) brGDGTs in the hypolimnion. Row labels indicate order names with relative abundance percentages across the whole lake. Symbols: "x" marks indicator species, calculated for the epilimnion and the hypolimnion ($p < 0.05$) and "+" indicates Pearson correlations with p value <0.1.

4. Discussion

4.1. Abiotic and Biotic Drivers of brGDGTs Production in the Lake Water Column

In Rotsee, seasonal stratification significantly influences brGDGT concentrations. Notable changes in brGDGT concentrations occur during the stratified summer months, coinciding with the epilimnion. Core lipid (CL) and intact polar lipid (IPL) brGDGT fractions show distinct temporal variations, suggesting independent production rather than a simple precursor-product relationship. For instance, elevated CL brGDGT Ia concentrations in the epilimnion occur without a corresponding IPL increase. Although IPL degradation to CLs has been shown to occur in the environment (Lengger et al., 2013; Raberg et al., 2022; Tierney et al., 2012), the lack of consistent correspondence between IPL and CL concentration indicates that additional processes, for example, in situ production of CLs, contribute to CL concentration changes. The occasional comparability between August hypolimnion IPL and November epilimnion CL brGDGTs distributions, potentially reflect either transport of lipids

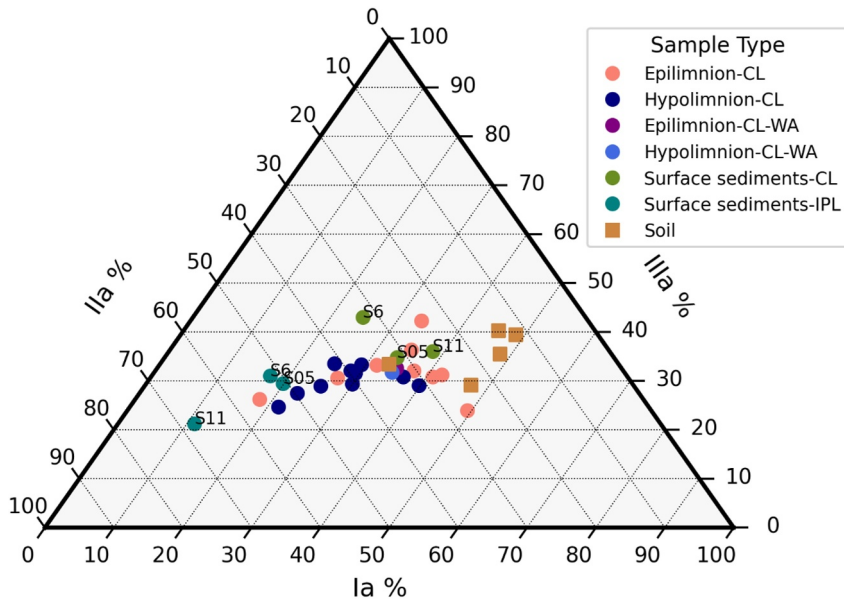

Figure 7. Ternary plot based on fractional abundances of the brGDGTs Ia, IIa, and IIIa and either core lipid (CL) or intact polar lipid (IPL) brGDGT distributions. The sum of the fractional abundances amounts to 100%. Color is used to distinguish the SPM sampling depth (epilimnion or hypolimnion, CL distribution), surface sediment (CL or IPL, the CL fractions are labeled in the plot), and soil samples. Weighted average (WA) of these fractional abundances of both the epilimnion and the hypolimnion are plotted in magenta and blue (see legend).

or transport of brGDGT-producing microbes during seasonal mixing. Overall, however, the repeated decoupling of CL and IPL concentrations in the water column supports partially independent production pathways for these lipid pools within the lake. While soil input could also theoretically contribute to the IPL/CL differences (Raberg et al., 2022), Rotsee soils are compositionally distinct (brGDGT Ia-dominated, lower IR; Figure 7) and soils generally show less pronounced seasonal variation than lakes (Naafs et al., 2017; Weijers et al., 2011). The direction of seasonal change in the lake also does not match a soil-derived signal, and inflow to small, sheltered lakes like Rotsee is typically reduced during stratification, making substantial seasonal soil pulses unlikely. This suggests that IPL degradation alone does not fully explain CL brGDGT dynamics and highlights the need for a separate discussion of their formation and transformation mechanisms.

Globally, the fractional abundance of brGDGT Ia increases with warmer temperatures, while brGDGT IIIa dominates in colder or deeper waters (Russell et al., 2018; Stefanescu et al., 2021; Weber et al., 2018; Yao et al., 2020). This pattern is partially evident in Rotsee, with a slight increase in CL brGDGT Ia concentrations in the epilimnion during the stratified month of July and increased brGDGT IIIa in the hypolimnion during cooler mixing periods, with notable increases also observed during stratified May and June (Figure 3). The 6-methyl brGDGT IIIa' is predominantly produced in the epilimnion during summer, supporting its role as an aquatic production marker (Ajallooeian et al., 2024b; De Jonge et al., 2014; Guo et al., 2020). IPL brGDGTs are produced in the anoxic hypolimnion, while epilimnion IPLs occur mainly during mixing seasons, suggesting transport from the hypolimnion during thermocline deepening rather than in situ production. Though nutrient-stimulated production or seasonal microbial shifts may also contribute (Loomis, Russell, Heureux, et al., 2014; van Bree et al., 2020), mixing is the most parsimonious explanation, and the low December epilimnion value of MBT'_{5ME} likely reflects seasonal temperature effects. This establishes distinct production zones with CL brGDGTs dominating epilimnion production and both CL and IPL brGDGTs produced in the hypolimnion. This depth segregation allows us to constrain bacterial producers for these different lipid groups in their respective environments.

Anoxic conditions appear critical for IPL brGDGT production in the hypolimnion, consistent with culture studies reporting enhanced production under oxygen limitation (Chen et al., 2022; Halamka et al., 2022). Similarly, other studies have shown that brGDGT production is shaped by stratification and redox conditions rather than temperature, with distinct microbial communities occupying different redox zones (van Bree et al., 2020; Weber

et al., 2018). In Rotsee, epilimnion IPLs only occur during mixing seasons, mirroring hypolimnion distributions with decreased brGDGT Ia and increased brGDGT IIIa (Figures 3c and 3d). In Rotsee, hexamethylated brGDGTs (IIIa and IIIa') dominate the IPL pool produced under anoxic conditions, a pattern also observed in other Swiss lakes (Weber et al., 2018). However, this pattern can vary regionally; for instance, Wu et al. (2021) found that 5-methyl brGDGT production (rather than 6-methyl brGDGT) was favored under anoxic conditions in surface sediments of the Chinese lake, Yangzonghai.

Overall, brGDGT production appears to be controlled by the water column structure, with epilimnetic temperature (onset of stratification) primarily influencing the upper water column compounds and oxygen availability governing those in the hypolimnion. This distinction challenges simple temperature interpretations of these proxies.

4.2. Environmental Drivers on brGDGTs Distribution

4.2.1. Proposed Temperature-Sensitive brGDGTs Ia, IIa, and IIIa and Their Ratios

In Rotsee, the composition of CL brGDGTs in the epilimnion and the hypolimnion exhibits depth-dependent variability, influenced by environmental factors such as temperature, conductivity, alkalinity, pH, and dissolved oxygen. Principal component analysis (PCA) shows that the first two principal components capture 67% of the variance in the epilimnion and 86% in the hypolimnion (Figure S3 in Supporting Information S1). Environmental parameters projected a posteriori onto the ordination indicate that these factors correlate with the main compositional gradients.

The fractional abundance of brGDGT Ia, widely interpreted as a temperature-sensitive compound (Raberg et al., 2021), increases during the warm summer months (Figures 3b and 4c). This is consistent with global observations linking increased brGDGT Ia fractional abundance to warmer temperatures in lake sediments (Martínez-Sosa et al., 2021; Raberg et al., 2021; Russell et al., 2018). Similarly, brGDGT Ib, another globally temperature-sensitive compound (e.g., Raberg et al., 2021), shows a positive correlation with temperature ($r = 0.61$ and $p < 0.05$). However, the fractional abundances of brGDGTs IIa and IIIa exhibit a negative correlation with temperature (Table S3). The impact of thermocline deepening and water column mixing during cooler seasons contributes to the observed yearly trends in brGDGT distribution. This needs to be considered when correlations between temperature and brGDGTs are evaluated. For example, in the epilimnion, brGDGT Ia fractional abundance, which is closely linked to temperature, declines during thermocline deepening (October–November) and full water column mixing (November–December). During these periods, hypolimnion-derived brGDGTs, such as IIIa, which are associated with mixing from deeper, cooler water, are transported into the epilimnion (Figure 3c). Notably, MBT'_{5ME} values in the epilimnion during poststratification (October–November) converge with those in the hypolimnion, indicating that the upward mixing of cooler, IIIa-enriched waters dampens any further temperature response. This convergence results in a weak overall correlation between MBT'_{5ME} and temperature ($r = 0.59$, $p = 0.10$), supporting the conclusion that the MBT'_{5ME} index in the epilimnion reflects both stratification dynamics and temperature variations, rather than temperature alone.

Additionally, MBT'_{5ME} in the epilimnion also correlates significantly with conductivity ($r = 0.71$ and $p < 0.05$), consistent with the seasonal rise in temperature and conductivity during stratification (Figure 2). For reference, MBT'_{5ME} increases from ~0.4 in winter to ~0.5 in early summer, paralleling a conductivity rise from ~150 to ~230 µS cm^{-1}, before both decline toward winter. This reflects the correlation ($r = 0.66$, $p < 0.05$) between temperature and conductivity, driven by evaporation and/or productivity based on global-scale analyses (Raberg et al., 2021), higher conductivity has been linked to shifts in brGDGT distributions. As MBT'_{5ME} is calculated from the fractional abundances of specific brGDGTs, such shifts could bias the temperature signal by altering the proportion of brGDGTs included in the index.

Although 6-methyl compounds are not traditionally associated with temperature sensitivity, an increased IIIa' fractional abundance (Figure 5) in response to warmer temperatures is notably visible in July. This temperature dependency of the fractional abundance of brGDGT IIIa' agrees with recent studies (Martínez-Sosa et al., 2020; Russell et al., 2018) that have observed positive correlations between the fractional abundances of brGDGTs IIa' and IIIa' and growth temperature in aquatic environments. Interestingly, the IR, as evident from Figure 5a, demonstrates a more robust correlation with temperature in epilimnion waters ($r = 0.68$ and $p < 0.05$) than MBT'_{5ME}. Furthermore, the stepwise forward selection analysis confirms temperature as the primary environmental control on the variance in IR in the epilimnion (explaining 46%, Table S2). Adding conductivity only

marginally increased the explained variance to 53%, while dissolved oxygen, pH, and alkalinity did not significantly contribute. These results indicate that although conductivity is linearly correlated with IR ($r = 0.65$ and $p < 0.05$), matching previous global observations (Raberg et al., 2021), temperature (with its large 17°C seasonal range) dominates the variability in brGDGTs distribution. This is supported by previous findings using mesocosm approaches or on large spatial scales (Ajallooeian et al., 2024b; Martínez-Sosa et al., 2020; Martínez-Sosa & Tierney, 2019). While recent work by Novak et al. (2025) reports a weak positive temperature dependency of the IR on the global scale, this study highlights that the temperature response potentially explains the largest part of the IR values in the lacustrine epilimnion. Nevertheless, the observed correlation between IR and conductivity further indicates that in lakes where variation in conductivity is temperature-dependent, distinguishing the direct influences of conductivity and/or temperature on IR can be challenging.

These results show that the distributions of brGDGTs Ia, IIa, and IIIa in Rotsee are shaped by both temperature and seasonal mixing, with thermocline dynamics weakening the direct temperature-MBT'$_{5ME}$ relationship. By contrast, the IR index provides a clearer temperature signal, though partly confounded by conductivity. Thus, in lake's epilimnion, temperature emerges as the dominant driver of brGDGT variability, while mixing processes and secondary conductivity effects modulate the apparent response.

4.2.2. Chemistry-Sensitive 6-Methyls and IR

In the Rotsee hypolimnion, dissolved oxygen (DO) appears to exert significant control over the production of 6-methyl CL-brGDGTs. Although the concentrations of individual 5- and 6-methyl brGDGTs do not directly correlate with DO, their fractional abundances, specifically those of cyclopentane-containing brGDGTs IIb, Ib, and Ic, as well as 6-methyl brGDGTs IIa' and IIb', show a strong negative correlation with DO ($r = -0.64$ to -0.80 and $p < 0.05$). Similarly, IR displays a negative correlation with DO ($r = -0.65$ and $p < 0.05$), as well as positive correlations with alkalinity ($r = 0.66$ and $p < 0.05$). These findings align with previous studies (e.g., Dang et al., 2018; Russell et al., 2018; van Bree et al., 2020; Weber et al., 2018; Wu et al., 2021), which have similarly reported an anticorrelation between IR and DO in anoxic environments. This relationship highlights the sensitivity of IR to oxygen depletion, consistent with observations from other stratified lakes, such as the Chinese warm monomictic lake Yangzonghai (Wu et al., 2021). In Lake Yangzonghai, the fractional abundance of 6-methyl brGDGTs and IR also showed a strong negative correlation with DO, reinforcing the interpretation that these compounds are preferentially produced under low-oxygen conditions.

Taken together, these results highlight the dual control of IR by temperature in the epilimnion and by dissolved oxygen and nutrient dynamics in the seasonally anoxic hypolimnion. While IR shows promise as a temperature proxy in the epilimnion, its sensitivity to DO and nutrients in the hypolimnion complicates its interpretation in stratified lakes.

4.3. Provenance of brGDGTs in Surface Sediments

Interpreting brGDGT distribution in lake sediments will not only represent an average signal of the overlying water column but also a potential contribution of watershed soils. The soil samples around Rotsee exhibit brGDGT distributions different from those in the lake surface sediments (Figure 7). Their higher MBT'$_{5ME}$ and lower IR values suggest minimal input of soil-derived brGDGTs into the lake, contrasting with the findings of Naeher et al. (2014), who suggested a more substantial soil contribution to the brGDGT pool in Rotsee. This difference likely reflects methodological advances and our broader data set, which includes seasonal water column and multidepth sediment records. A second source is in situ production by bacteria living within the surface sediments. If this production were absent, the lacustrine sediments would represent a mixture of epilimnion and hypolimnion brGDGTs. However, while the shallow and intermediate sediments are expected to receive brGDGTs originating from the epilimnion, an average MBT'$_{5ME}$ signal of 0.33 (calculated as the mean of 0.26 and 0.40) is observed, which reflects a colder sediment signal potentially indicating sedimentary production. In the deepest sediment (11 m depth), the brGDGT concentration peaks, consistent with previous studies (van Bree et al., 2020; Weber et al., 2018). Here, the MBT'$_{5ME}$ signal (0.44) reflects a combined contribution from epilimnion and hypolimnion, though the fractional abundance of brGDGTs Ia, IIa, and IIIa closely resemble an epilimnion-derived signal (Figure 7). This yields a reconstructed temperature based on water column brGDGT distribution that is 2°C higher than the value derived from the full water column data set but is in line with measured regional MAAT (14°C). Sedimentary IPL brGDGTs, shown by their strong and distinct IPL signature

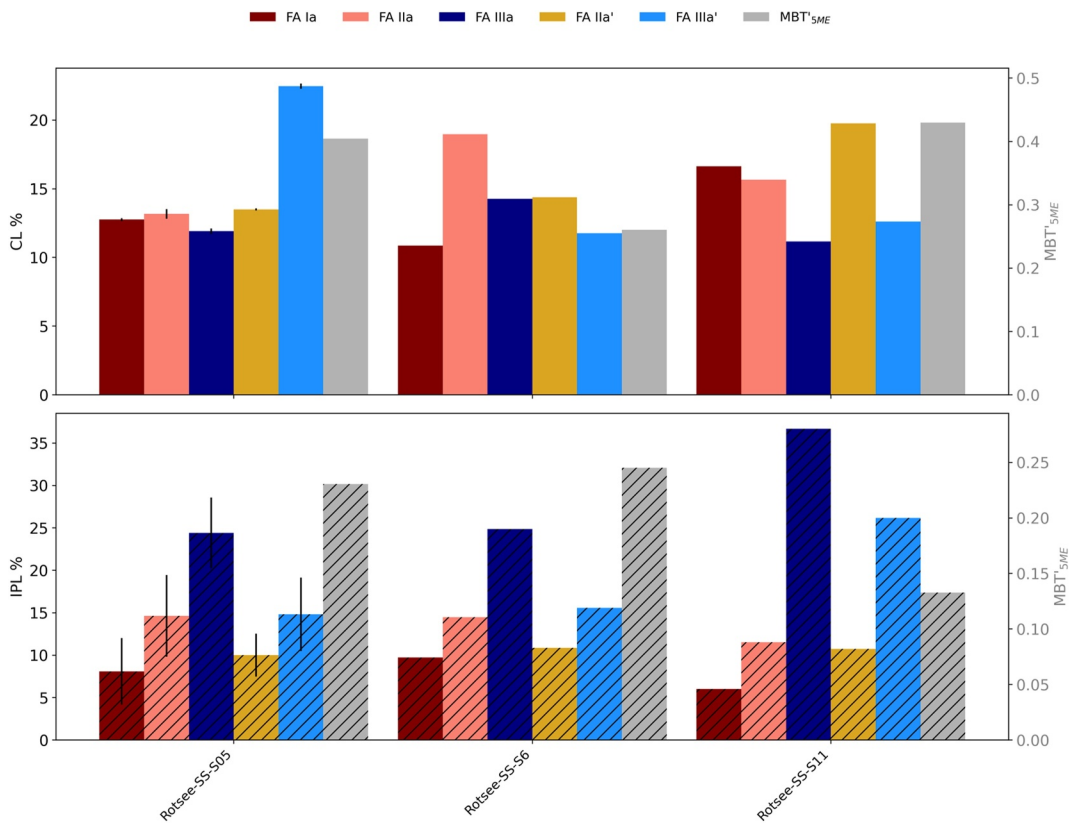

Figure 8. The fractional abundances (left *y*-axis) and MBT'$_{5ME}$ (right *y*-axis) of CL and IPL brGDGTs in the surface sediment samples of Rotsee. The error bars represent the standard deviation between the 2 shallow sediments analyzed for the S05 sample. Station codes (S0.5, S6, and S11) indicate the water depth (in meters) at which the surface sediment sample was collected.

indicate in situ production, yet they do not alter the CL distribution (Figure 7, Table S1). In the deepest sediments, IPL brGDGTs exhibit lower MBT'$_{5ME}$ and higher abundances of IIIa and IIIa', suggesting a different source or production mechanism compared to shallower sediments with higher IPL GDGT-based MBT'$_{5ME}$ (Figure 8). Although colder deep water temperatures could contribute to the elevated IIIa and IIIa', their cooccurrence with anoxia and strong IPL signatures, and similar patterns reported as temperature-independent in other lakes (Stefanescu et al., 2021), point to redox-driven production or transport as more likely explanations.

Still, the environmental dependency of the smaller differences within the sedimentary MBT'$_{5ME}$ values (0.26 vs. 0.44) should not be overinterpreted, particularly given the large range in MBT'$_{5ME}$ values previously reported in single lake systems (Wu et al., 2021). This suggests that lake depth alone does not reliably indicate whether sedimentary brGDGTs originate from the water column or are produced in situ within the sediments.

Based on the in-depth study of the Rotsee water column, we propose that a strong correlation between MBT'$_{5ME}$ and IR in sedimentary archives, similar to the correlation observed in the Rotsee epilimnion ($r = 0.93$ and $p < 0.0001$; Figure 5, Figure S2 in Supporting Information S1), may serve as an indicator of brGDGTs predominantly sourced from the surface waters. This correlation arises because Ia, (IIa + IIIa), and (IIa'+IIIa') vary together as a linked three-component compositional system in the epilimnion. Coordinated shifts among these compounds define a directional gradient in brGDGT distributions along which both MBT'$_{5ME}$ and IR change (Figure S4 in Supporting Information S1). In contrast, this structured covariation is not present in the hypolimnion, where the two indices vary independently. This indicates that the MBT'$_{5ME}$-IR relationship observed in the epilimnion reflects environmentally driven changes in brGDGT production. Hence, by reflecting epilimnion conditions, we propose that when this correlation between MBT'$_{5ME}$ and IR is observed in sedimentary records, it can increase confidence in using MBT'$_{5ME}$ for paleotemperature reconstructions. Conversely, a lack of agreement

may suggest additional environmental controls, a stronger hypolimnion contribution, or sedimentary in situ production, warranting caution in proxy interpretation.

5. Conclusions

This study examined how environmental factors influence brGDGT production and deposition in Rotsee, a seasonally stratified lake, to refine their application as paleoclimate proxies. Seasonal stratification is the dominant influence, regulating both depth-specific production of brGDGTs and their eventual sedimentary signal. Bacterial community analysis further indicates that brGDGT production extends beyond Acidobacteria, with stronger associations observed between hypolimnion IPLs and multiple bacterial orders, highlighting the role of diverse microbial contributors.

Distinct production patterns were observed for core lipids (CL) and intact polar lipids (IPL). While CL brGDGTs were produced throughout the water column, including in oxic environments; IPL production is concentrated in the anoxic hypolimnion. These findings highlight that stratification dynamics must be considered when interpreting brGDGT distributions, as they modulate both production depth and sedimentary transfer.

Surface sediments show negligible soil-derived brGDGT input, with evidence for in situ IPL-brGDGTs production that does not strongly alter CL distributions at the depths examined. However, future work on paired IPL-CL measurements in sediment cores will be important to resolve the role of IPL degradation in shaping downcore brGDGT distributions. Deeper sediments beneath the anoxic hypolimnion most closely reflect an integrated water column signal, while shallow oxic sediments exhibit additional CL production. These patterns not only support the use of deep sediments for reconstructing lake-wide signals but also highlight the potential for diagenetic overprints, underscoring the need for targeted IPL-CL studies in sediment cores to refine GDGT-based paleoclimate reconstructions.

A particularly novel outcome of this study is the strong correlation between the MBT'_{5ME} and IR in the epilimnion of Rotsee. We propose this relationship as a diagnostic tool for identifying brGDGTs sourced predominantly from surface waters, and for disentangling epilimnion versus hypolimnion contributions in sedimentary records. Given that many environmental dependencies in Rotsee align with global patterns, this methodology holds promise for broader application in thermally stratified lakes with isolated hypolimnion zones.

Taken together, our results underscore four key insights: (a) stratification-dependent environmental controls strongly shape brGDGT production and deposition, (b) MBT'_{5ME}-IR correlation offers a novel diagnostic tool to trace source contributions, (c) microbial diversity likely underpins brGDGT production beyond Acidobacteria, and (d) these findings have direct implications for the robustness and interpretation of paleoclimate proxies in seasonally stratified lakes.

Conflict of Interest

The authors declare no conflicts of interest relevant to this study.

Data Availability Statement

The data sets supporting this study include brGDGT concentrations and environmental data from Rotsee (Ajallooeian et al., 2024c) and 16S rRNA gene sequences from Rotsee suspended particulate matter (Ajallooeian et al., 2024a).

Acknowledgments
This work was supported by the Swiss National Science Foundation [SNSF Project MiCoDy, grant PR00P2_179783]. In addition, the authors wish to express their gratitude for the assistance provided during the fieldwork of this project by Patrick Kathriner, Karin Beck, Nina Studhalter, Sandra Schmid, and Alois Zwyssig and for the valuable support extended by the staff of the Genetic Diversity Center of ETH Zürich (GDC) in the microbiological laboratory work. Open access publishing facilitated by Eidgenossische Technische Hochschule Zurich, as part of the Wiley - Eidgenossische Technische Hochschule Zurich agreement via the Consortium Of Swiss Academic Libraries.

References

Ajallooeian, F., Deng, L., Lever, M. A., & De Jonge, C. (2024a). 16S rRNA gene sequences from Rotsee suspended particulate matter [Dataset]. *NCBI Sequence Read Archive*. https://www.ncbi.nlm.nih.gov/bioproject/PRJNA1191886

Ajallooeian, F., Deng, L., Lever, M. A., & De Jonge, C. (2024b). Seasonal temperature dependency of aquatic branched glycerol dialkyl glycerol tetraethers: A mesocosm approach. *Organic Geochemistry*, *189*, 104742. https://doi.org/10.1016/j.orggeochem.2024.104742

Ajallooeian, F., Dubois, N., Ladd, S. N., Lever, M. A., Schubert, C. J., & De Jonge, C. (2024c). Controls on brGDGT production in the seasonally anoxic water column and sediments of Rotsee - Complete dataset [Dataset]. *ETH Zurich Research Collection*. https://doi.org/10.3929/ethz-b-000696997

Baxter, A. J., Peterse, F., Verschuren, D., & Sinninghe Damsté, J. S. (2024). Assessment of branched glycerol monoalkyl glycerol tetraether (brGMGT)-based paleothermometry in the 250,000-year sediment record of Lake Chala, equatorial East Africa. *Organic Geochemistry*, *195*, 104812. https://doi.org/10.1016/j.orggeochem.2024.104812

Bechtel, A., Smittenberg, R. H., Bernasconi, S. M., & Schubert, C. J. (2010). Distribution of branched and isoprenoid tetraether lipids in an oligotrophic and a eutrophic Swiss lake: Insights into sources and GDGT-based proxies. *Organic Geochemistry*, *41*(8), 822–832. https://doi.org/10.1016/j.orggeochem.2010.04.022

Berg, J. S., Lepine, M., Laymand, E., Han, X., Vogel, H., Morlock, M. A., et al. (2022). Ancient and modern geochemical signatures in the 13,500-year sedimentary record of Lake Cadagno. *Frontiers in Earth Science*, *9*, 754888. https://doi.org/10.3389/feart.2021.754888

Blanchet, F. G., Legendre, P., & Borcard, D. (2008). Forward selection of explanatory variables. *Ecology*, *89*(9), 2623–2632. https://doi.org/10.1890/07-0986.1

Buckles, L. K., Weijers, J. W., Verschuren, D., & Sinninghe Damsté, J. S. (2014). Sources of core and intact branched tetraether membrane lipids in the lacustrine environment: Anatomy of Lake Challa and its catchment, equatorial East Africa. *Geochimica et Cosmochimica Acta*, *140*, 106–126. https://doi.org/10.1016/j.gca.2014.04.042

Chen, Y., Zheng, F., Yang, H., Yang, W., Wu, R., Liu, X., et al. (2022). The production of diverse brGDGTs by an Acidobacterium providing a physiological basis for paleoclimate proxies. *Geochimica et Cosmochimica Acta*, *337*, 155–165. https://doi.org/10.1016/j.gca.2022.08.033

Colcord, D. E., Pearson, A., & Brassell, S. C. (2017). Carbon isotopic composition of intact branched GDGT core lipids in Greenland lake sediments and soils. *Organic Geochemistry*, *110*, 25–32. https://doi.org/10.1016/j.orggeochem.2017.04.008

Crampton-Flood, E. D., Tierney, J. E., Peterse, F., Kirkels, F. M., & Sinninghe Damsté, J. S. (2020). BayMBT: A Bayesian calibration model for branched glycerol dialkyl glycerol tetraethers in soils and peats. *Geochimica et Cosmochimica Acta*, *268*, 142–159. https://doi.org/10.1016/j.gca.2019.09.043

Dang, X., Ding, W., Yang, H., Pancost, R. D., Naafs, B. D. A., Xue, J., et al. (2018). Different temperature dependence of the bacterial brGDGT isomers in 35 Chinese lake sediments compared to that in soils. *Organic Geochemistry*, *119*, 72–79. https://doi.org/10.1016/j.orggeochem.2018.02.008

Davis, N. M., Proctor, D. M., Holmes, S. P., Relman, D. A., & Callahan, B. J. (2018). Simple statistical identification and removal of contaminant sequences in marker-gene and metagenomics data. *Microbiome*, *6*, 1–14. https://doi.org/10.1186/s40168-018-0605-2

De Cáceres, M. (2013). *How to use the indicspecies package*. (ver. 1.7. 1) (Vol. 29). R Proj.

Dedysh, S. N., & Sinninghe Damsté, J. S. (2018). Acidobacteria. *eLS*, 1–10. https://doi.org/10.1002/9780470015902.a0027685

De Jonge, C., Guo, J., Hällberg, P., Griepentrog, M., Rifai, H., Richter, A., et al. (2024). The impact of soil chemistry, moisture and temperature on branched and isoprenoid GDGTs in soils: A study using six globally distributed elevation transects. *Organic Geochemistry*, *187*, 104706. https://doi.org/10.1016/j.orggeochem.2023.104706

De Jonge, C., Hopmans, E. C., Zell, C. I., Kim, J. H., Schouten, S., & Sinninghe Damsté, J. S. (2014). Occurrence and abundance of 6-methyl branched glycerol dialkyl glycerol tetraethers in soils: Implications for palaeoclimate reconstruction. *Geochimica et Cosmochimica Acta*, *141*, 97–112. https://doi.org/10.1016/j.gca.2014.06.013

De Jonge, C., Kuramae, E. E., Radujković, D., Weedon, J. T., Janssens, I. A., & Peterse, F. (2021). The influence of soil chemistry on branched tetraether lipids in mid-and high latitude soils: Implications for brGDGT-based paleothermometry. *Geochimica et Cosmochimica Acta*, *310*, 95–112. https://doi.org/10.1016/j.gca.2021.06.037

De Jonge, C., Radujković, D., Sigurdsson, B. D., Weedon, J. T., Janssens, I., & Peterse, F. (2019). Lipid biomarker temperature proxy responds to abrupt shift in the bacterial community composition in geothermally heated soils. *Organic Geochemistry*, *137*, 103897. https://doi.org/10.1016/j.orggeochem.2019.07.006

Deng, L., Bölsterli, D., Kristensen, E., Meile, C., Su, C. C., Bernasconi, S. M., et al. (2020). Macrofaunal control of microbial community structure in continental margin sediments. *Proceedings of the National Academy of Sciences*, *117*(27), 15911–15922. https://doi.org/10.1073/pnas.1917494117

Dray, S., Legendre, P., & Peres-Neto, P. R. (2006). Spatial modelling: A comprehensive framework for principal coordinate analysis of neighbour matrices (PCNM). *Ecological Modelling*, *196*(3–4), 483–493. https://doi.org/10.1016/j.ecolmodel.2006.02.015

Guo, J., Glendell, M., Meersmans, J., Kirkels, F., Middelburg, J. J., & Peterse, F. (2020). Assessing branched tetraether lipids as tracers of soil organic carbon transport through the Carminowe Creek catchment (southwest England). *Biogeosciences*, *17*(12), 3183–3201. https://doi.org/10.5194/bg-17-3183-2020

Halamka, T. A., Raberg, J. H., McFarlin, J. M., Younkin, A. D., Mulligan, C., Liu, X. L., & Kopf, S. H. (2022). Production of diverse brGDGTs by Acidobacterium Solibacter usitatus in response to temperature, pH, and O2 provides a culturing perspective on br GDGT proxies and biosynthesis. *Geobiology*, *21*(1), 102–118. https://doi.org/10.1111/gbi.12525

Halffman, R., Lembrechts, J., Radujković, D., De Gruyter, J., Nijs, I., & De Jonge, C. (2022). Soil chemistry, temperature, and bacterial community composition drive brGDGT distributions along a subarctic elevation gradient. *Organic Geochemistry*, *163*, 104346. https://doi.org/10.1016/j.orggeochem.2021.104346

Han, X., Schubert, C. J., Fiskal, A., Dubois, N., & Lever, M. A. (2020). Eutrophication as a driver of microbial community structure in lake sediments. *Environmental Microbiology*, *22*(8), 3446–3462. https://doi.org/10.1111/1462-2920.15115

Hopmans, E. C., Schouten, S., & Sinninghe Damsté, J. S. (2016). The effect of improved chromatography on GDGT-based palaeoproxies. *Organic Geochemistry*, *93*, 1–6. https://doi.org/10.1016/j.orggeochem.2015.12.006

Hu, J., Zhou, H., & Spiro, B. (2016). Seasonal variability in concentrations and fluxes of glycerol dialkyl glycerol tetraethers in Huguangyan Maar Lake, SE China: Implications for the applicability of the MBT–CBT paleotemperature proxy in lacustrine settings. *Chemical Geology*, *420*, 200–212. https://doi.org/10.1016/j.chemgeo.2015.11.008

Huguet, C., Hopmans, E. C., Febo-Ayala, W., Thompson, D. H., Sinninghe Damsté, J. S., & Schouten, S. (2006). An improved method to determine the absolute abundance of glycerol dibiphytanyl glycerol tetraether lipids. *Organic Geochemistry*, *37*(9), 1036–1041. https://doi.org/10.1016/j.orggeochem.2006.05.008

Huguet, C., Martens-Habbena, W., Urakawa, H., Stahl, D. A., & Ingalls, A. E. (2010). Comparison of extraction methods for quantitative analysis of core and intact polar glycerol dialkyl glycerol tetraethers (BrGDGTs) in environmental samples. *Limnology and Oceanography: Methods*, *8*(4), 127–145. https://doi.org/10.4319/lom.2010.8.127

Kaufman, D., McKay, N., Routson, C., Erb, M., Davis, B., Heiri, O., et al. (2020). Holocene global mean surface temperature, a multi-method reconstruction approach. *Scientific Data*, *7*(1), 201. https://doi.org/10.1038/s41597-020-0530-7

Legendre, P., & Legendre, L. (2012). *Numerical ecology*. Elsevier.

Lengger, S. K., Kraaij, M., Tjallingii, R., Baas, M., Stuut, J. B., Hopmans, E. C., et al. (2013). Differential degradation of intact polar and core glycerol dialkyl glycerol tetraether lipids upon post-depositional oxidation. *Organic Geochemistry*, *65*, 83–93. https://doi.org/10.1016/j.orggeochem.2013.10.004

Lever, M. A., Torti, A., Eickenbusch, P., Michaud, A. B., Šantl-Temkiv, T., & Jørgensen, B. B. (2015). A modular method for the extraction of DNA and RNA, and the separation of DNA pools from diverse environmental sample types. *Frontiers in Microbiology*, *6*, 476. https://doi.org/10.3389/fmicb.2015.00476

Loomis, S. E., Russell, J. M., Eggermont, H., Verschuren, D., & Sinninghe Damsté, J. S. (2014). Effects of temperature, pH and nutrient concentration on branched GDGT distributions in East African lakes: Implications for paleoenvironmental reconstruction. *Organic Geochemistry*, *66*, 25–37. https://doi.org/10.1016/j.orggeochem.2013.10.012

Loomis, S. E., Russell, J. M., Heureux, A. M., D'Andrea, W. J., & Sinninghe Damsté, J. S. (2014). Seasonal variability of branched glycerol dialkyl glycerol tetraethers (brGDGTs) in a temperate lake system. *Geochimica et Cosmochimica Acta*, *144*, 173–187. https://doi.org/10.1016/j.gca.2014.08.027

Loomis, S. E., Russell, J. M., Ladd, B., Street-Perrott, F. A., & Sinninghe Damsté, J. S. (2012). Calibration and application of the branched GDGT temperature proxy on East African lake sediments. *Earth and Planetary Science Letters*, *357*, 277–288. https://doi.org/10.1016/j.epsl.2012.09.031

Martínez-Sosa, P., & Tierney, J. E. (2019). Lacustrine brGDGT response to microcosm and mesocosm incubations. *Organic Geochemistry*, *127*, 12–22. https://doi.org/10.1016/j.orggeochem.2018.10.011

Martínez-Sosa, P., Tierney, J. E., & Meredith, L. K. (2020). Controlled lacustrine microcosms show a brGDGT response to environmental perturbations. *Organic Geochemistry*, *145*, 104041. https://doi.org/10.1016/j.orggeochem.2020.104041

Martínez-Sosa, P., Tierney, J. E., Stefanescu, I. C., Crampton-Flood, E. D., Shuman, B. N., & Routson, C. (2021). A global Bayesian temperature calibration for lacustrine brGDGTs. *Geochimica et Cosmochimica Acta*, *305*, 87–105. https://doi.org/10.1016/j.gca.2021.04.038

Masion, A., Vilgé-Ritter, A., Rose, J., Stone, W. E., Teppen, B. J., Rybacki, D., & Bottero, J. Y. (2000). Coagulation-flocculation of natural organic matter with Al salts: Speciation and structure of the aggregates. *Environmental Science and Technology*, *34*(15), 3242–3246.

McMurdie, P. J., & Holmes, S. (2013). Phyloseq: An R package for reproducible interactive analysis and graphics of microbiome census data. *PLoS One*, *8*(4), e61217. https://doi.org/10.1371/journal.pone.0061217

Miller, D. R., Habicht, M. H., Keisling, B. A., Castañeda, I. S., & Bradley, R. S. (2018). A 900-year New England temperature reconstruction from in situ seasonally produced branched glycerol dialkyl glycerol tetraethers (brGDGTs). *Climate of the Past*, *14*(11), 1653–1667. https://doi.org/10.5194/cp-14-1653-2018

Naafs, B. D. A., Gallego-Sala, A. V., Inglis, G. N., & Pancost, R. D. (2017). Refining the global branched glycerol dialkyl glycerol tetraether (brGDGT) soil temperature calibration. *Organic Geochemistry*, *106*, 48–56. https://doi.org/10.1016/j.orggeochem.2017.01.009

Naafs, B. D. A., Oliveira, A. S. F., & Mulholland, A. J. (2021). Molecular dynamics simulations support the hypothesis that the brGDGT paleothermometer is based on homeoviscous adaptation. *Geochimica et Cosmochimica Acta*, *312*, 44–56. https://doi.org/10.1016/j.gca.2021.07.034

Naeher, S., Peterse, F., Smittenberg, R. H., Niemann, H., Zigah, P. K., & Schubert, C. J. (2014). Sources of glycerol dialkyl glycerol tetraethers (BrGDGTs) in catchment soils, water column and sediments of Rotsee(Switzerland)–Implications for the application of GDGT-based proxies for lakes. *Organic Geochemistry*, *66*, 164–173. https://doi.org/10.1016/j.orggeochem.2013.10.017

Novak, J. B., Russell, J. M., Lindemuth, E. R., Prokopenko, A. A., Pérez-Angel, L., Zhao, B., et al. (2025). The branched GDGT isomer ratio refines lacustrine paleotemperature estimates. *Geochemistry, Geophysics, Geosystems*, *26*(3), e2024GC012069. https://doi.org/10.1029/2024gc012069

O'Beirne, M. D., Vornlocher, J. R., Lopera-Congote, L., Emordi, E. E., Ubit, G., Contreras, S., et al. (2025). Exploring the influence of temperature on brGDGT distributions in Chilean Lakes and soils: A comparative analysis of in situ measured and modeled temperature data. *Journal of Geophysical Research: Biogeosciences*, *130*(7), e2024JG008506. https://doi.org/10.1029/2024jg008506

Oksanen, J., Blanchet, F. G., Kindt, R., Legendre, P., Minchin, P. R., O'hara, R. B., et al. (2013). Package "vegan". Community ecology package, version, *2*(9), 1–295.

Peterse, F., Kim, J. H., Schouten, S., Kristensen, D. K., Koç, N., & Sinninghe Damsté, J. S. (2009). Constraints on the application of the MBT/CBT palaeothermometer at high latitude environments (Svalbard, Norway). *Organic Geochemistry*, *40*(6), 692–699. https://doi.org/10.1016/j.orggeochem.2009.03.004

Peterse, F., Nicol, G. W., Schouten, S., & Sinninghe Damsté, J. S. (2010). Influence of soil pH on the abundance and distribution of core and intact polar lipid-derived branched BrGDGTs in soil. *Organic Geochemistry*, *41*(10), 1171–1175. https://doi.org/10.1016/j.orggeochem.2010.07.004

Peterse, F., van der Meer, J., Schouten, S., Weijers, J. W., Fierer, N., Jackson, R. B., et al. (2012). Revised calibration of the MBT–CBT paleotemperature proxy based on branched tetraether membrane lipids in surface soils. *Geochimica et Cosmochimica Acta*, *96*, 215–229. https://doi.org/10.1016/j.gca.2012.08.011

Pitcher, A., Hopmans, E. C., Schouten, S., & Sinninghe Damsté, J. S. (2009). Separation of core and intact polar archaeal tetraether lipids using silica columns: Insights into living and fossil biomass contributions. *Organic Geochemistry*, *40*(1), 12–19. https://doi.org/10.1016/j.orggeochem.2008.09.008

Raberg, J. H., Flores, E., Crump, S. E., de Wet, G., Dildar, N., Miller, G. H., et al. (2022). Intact polar brGDGTs in Arctic lake catchments: Implications for lipid sources and paleoclimate applications. *Journal of Geophysical Research: Biogeosciences*, *127*(10), e2022JG006969. https://doi.org/10.1029/2022jg006969

Raberg, J. H., Harning, D. J., Crump, S. E., de Wet, G., Blumm, A., Kopf, S., et al. (2021). Revised fractional abundances and warm-season temperatures substantially improve brGDGT calibrations in lake sediments. *Biogeosciences*, *18*(12), 3579–3603. https://doi.org/10.5194/bg-18-3579-2021

Ramos-Roman, M. J., De Jonge, C., Magyari, E., Veres, D., Ilvonen, L., Develle, A. L., & Seppä, H. (2022). Lipid biomarker (brGDGT)-and pollen-based reconstruction of temperature change during the middle to late Holocene transition in the Carpathians. *Global and Planetary Change*, *215*, 103859. https://doi.org/10.1016/j.gloplacha.2022.103859

Rodriguez, P., Berg, J. S., Deng, L., Vogel, H., Okoniewski, M., Lever, M. A., & Magnabosco, C. (2025). Persistent functional and taxonomic groups dominate an 8,000-year sedimentary sequence from Lake Cadagno, Switzerland. *Frontiers in Microbiology*, *16*, 1504355. https://doi.org/10.3389/fmicb.2025.1504355

Russell, J. M., Hopmans, E. C., Loomis, S. E., Liang, J., & Sinninghe Damsté, J. S. (2018). Distributions of 5-and 6-methyl branched glycerol dialkyl glycerol tetraethers (brGDGTs) in East African lake sediment: Effects of temperature, pH, and new lacustrine paleotemperature calibrations. *Organic Geochemistry*, *117*, 56–69. https://doi.org/10.1016/j.orggeochem.2017.12.003

Sahonero-Canavesi, D. X., Siliakus, M. F., Abdala Asbun, A., Koenen, M., von Meijenfeldt, F. B., Boeren, S., et al. (2022). Disentangling the lipid divide: Identification of key enzymes for the biosynthesis of membrane-spanning and ether lipids in Bacteria. *Science Advances*, *8*(50), eabq8652. https://doi.org/10.1126/sciadv.abq8652

Salter, S. J., Cox, M. J., Turek, E. M., Calus, S. T., Cookson, W. O., Moffatt, M. F., et al. (2014). Reagent and laboratory contamination can critically impact sequence-based microbiome analyses. *BMC Biology*, *12*, 1–12. https://doi.org/10.1186/s12915-014-0087-z

Schoon, P. L., De Kluijver, A., Middelburg, J. J., Downing, J. A., Sinninghe Damsté, J. S., & Schouten, S. (2013). Influence of lake water pH and alkalinity on the distribution of core and intact polar branched glycerol dialkyl glycerol tetraethers (BrGDGTs) in lakes. *Organic Geochemistry*, *60*, 72–82. https://doi.org/10.1016/j.orggeochem.2013.04.015

Schouten, S., Hopmans, E. C., & Sinninghe Damsté, J. S. (2013). The organic geochemistry of glycerol dialkyl glycerol tetraether lipids: A review. *Organic Geochemistry*, *54*, 19–61. https://doi.org/10.1016/j.orggeochem.2012.09.006

Schubert, C. J., Lucas, F. S., Durisch-Kaiser, E., Stierli, R., Diem, T., Scheidegger, O., et al. (2010). Oxidation and emission of methane in a monomictic lake (Rotseesee, Switzerland). *Aquatic Sciences*, *72*(4), 455–466. https://doi.org/10.1007/s00027-010-0148-5

Sheik, C. S., Reese, B. K., Twing, K. I., Sylvan, J. B., Grim, S. L., Schrenk, M. O., et al. (2018). Identification and removal of contaminant sequences from ribosomal gene databases: Lessons from the census of deep life. *Frontiers in Microbiology*, *9*, 840. https://doi.org/10.3389/fmicb.2018.00840

Sinninghe Damsté, J. S., Hopmans, E. C., Pancost, R. D., Schouten, S., & Geenevasen, J. A. (2000). Newly discovered non-isoprenoid glycerol dialkyl glycerol tetraether lipids in sediments. *Chemical Communications*(17), 1683–1684. https://doi.org/10.1039/b004517i

Stefanescu, I. C., Shuman, B. N., & Tierney, J. E. (2021). Temperature and water depth effects on brGDGT distributions in sub-alpine lakes of mid-latitude North America. *Organic Geochemistry*, *152*, 104174. https://doi.org/10.1016/j.orggeochem.2020.104174

Sturt, H. F., Summons, R. E., Smith, K., Elvert, M., & Hinrichs, K. U. (2004). Intact polar membrane lipids in prokaryotes and sediments deciphered by high-performance liquid chromatography/electrospray ionization multistage mass spectrometry—new biomarkers for biogeochemistry and microbial ecology. *Rapid Communications in Mass Spectrometry*, *18*(6), 617–628. https://doi.org/10.1002/rcm.1378

Tierney, J. E., & Russell, J. M. (2009). Distributions of branched BrGDGTs in a tropical lake system: Implications for lacustrine application of the MBT/CBT paleoproxy. *Organic Geochemistry*, *40*(9), 1032–1036. https://doi.org/10.1016/j.orggeochem.2009.04.014

Tierney, J. E., Schouten, S., Pitcher, A., Hopmans, E. C., & Damsté Sinninghe, J. S. (2012). Core and intact polar glycerol dialkyl glycerol tetraethers (GDGTs) in Sand Pond, Warwick, Rhode Island (USA): Insights into the origin of lacustrine GDGTs. *Geochimica et Cosmochimica Acta*, *77*, 561–581. https://doi.org/10.1016/j.gca.2011.10.018

van Bree, L. G., Peterse, F., Baxter, A. J., De Crop, W., Van Grinsven, S., Villanueva, L., et al. (2020). Seasonal variability and sources of in situ brGDGT production in a permanently stratified African crater lake. *Biogeosciences*, *17*(21), 5443–5463. https://doi.org/10.5194/bg-17-5443-2020

Wang, H., Liu, W., He, Y., Zhou, A., Zhao, H., Liu, H., et al. (2021). Salinity-controlled isomerization of lacustrine brGDGTs impacts the associated MBT5ME'terrestrial temperature index. *Geochimica et Cosmochimica Acta*, *305*, 33–48. https://doi.org/10.1016/j.gca.2021.05.004

Watson, B. I., Williams, J. W., Russell, J. M., Jackson, S. T., Shane, L., & Lowell, T. V. (2018). Temperature variations in the southern Great Lakes during the last deglaciation: Comparison between pollen and GDGT proxies. *Quaternary Science Reviews*, *182*, 78–92. https://doi.org/10.1016/j.quascirev.2017.12.011

Weber, Y., Sinninghe Damsté, J. S., Hopmans, E. C., Lehmann, M. F., & Niemann, H. (2017). Incomplete recovery of intact polar glycerol dialkyl glycerol tetraethers from lacustrine suspended biomass. *Limnology and Oceanography: Methods*, *15*(9), 782–793. https://doi.org/10.1002/lom3.10198

Weber, Y., Sinninghe Damsté, J. S., Zopfi, J., De Jonge, C., Gilli, A., Schubert, C. J., et al. (2018). Redox-dependent niche differentiation provides evidence for multiple bacterial sources of glycerol tetraether lipids in lakes. *Proceedings of the National Academy of Sciences*, *115*(43), 10926–10931. https://doi.org/10.1073/pnas.1805186115

Weijers, J. W., Bernhardt, B., Peterse, F., Werne, J. P., Dungait, J. A., Schouten, S., & Sinninghe Damsté, J. S. (2011). Absence of seasonal patterns in MBT–CBT indices in mid-latitude soils. *Geochimica et Cosmochimica Acta*, *75*(11), 3179–3190. https://doi.org/10.1016/j.gca.2011.03.015

Weijers, J. W., Panoto, E., van Bleijswijk, J., Schouten, S., Rijpstra, W. I. C., Balk, M., et al. (2009). Constraints on the biological source (s) of the orphan branched tetraether membrane lipids. *Geomicrobiology Journal*, *26*(6), 402–414. https://doi.org/10.1080/01490450902937293

Weijers, J. W., Schefuß, E., Schouten, S., & Sinninghe Damsté, J. S. (2007). Coupled thermal and hydrological evolution of tropical Africa over the last deglaciation. *Science*, *315*(5819), 1701–1704. https://doi.org/10.1126/science.1138131

Weijers, J. W., Schouten, S., Hopmans, E. C., Geenevasen, J. A., David, O. R., Coleman, J. M., et al. (2006). Membrane lipids of mesophilic anaerobic bacteria thriving in peats have typical archaeal traits. *Environmental Microbiology*, *8*(4), 648–657. https://doi.org/10.1111/j.1462-2920.2005.00941.x

Weijers, J. W., Schouten, S., van den Donker, J. C., Hopmans, E. C., & Sinninghe Damsté, J. S. (2007). Environmental controls on bacterial tetraether membrane lipid distribution in soils. *Geochimica et Cosmochimica Acta*, *71*(3), 703–713. https://doi.org/10.1016/j.gca.2006.10.003

Weijers, J. W. H., Wiesenberg, G. L., Bol, R., Hopmans, E. C., & Pancost, R. D. (2010). Carbon isotopic composition of branched tetraether membrane lipids in soils suggest a rapid turnover and a heterotrophic life style of their source organism (s). *Biogeosciences*, *7*(9), 2959–2973. https://doi.org/10.5194/bg-7-2959-2010

Wu, J., Yang, H., Pancost, R. D., Naafs, B. D. A., Qian, S., Dang, X., et al. (2021). Variations in dissolved O2 in a Chinese lake drive changes in microbial communities and impact sedimentary GDGT distributions. *Chemical Geology*, *579*, 120348. https://doi.org/10.1016/j.chemgeo.2021.120348

Wu, J., Yang, H., Shen, C., Zhu, L., Pei, H., Dang, X., et al. (2023). BrGDGT-based quantitative reconstructions of paleotemperature in lakes: Regional vs. site-specific calibrations. *Quaternary Science Reviews*, *322*, 108416. https://doi.org/10.1016/j.quascirev.2023.108416

Yao, Y., Zhao, J., Vachula, R. S., Werne, J. P., Wu, J., Song, X., & Huang, Y. (2020). Correlation between the ratio of 5-methyl hexamethylated to pentamethylated branched BrGDGTs (HP5) and water depth reflects redox variations in stratified lakes. *Organic Geochemistry*, *147*, 104076. https://doi.org/10.1016/j.orggeochem.2020.104076

Zell, C., Kim, J. H., Moreira-Turcq, P., Abril, G., Hopmans, E. C., Bonnet, M. P., et al. (2013). Disentangling the origins of branched tetraether lipids and crenarchaeol in the lower Amazon River: Implications for GDGT-based proxies. *Limnology & Oceanography*, *58*(1), 343–353. https://doi.org/10.4319/lo.2013.58.1.0343

Zeng, Z., Chen, H., Yang, H., Chen, Y., Yang, W., Feng, X., et al. (2022). Identification of a protein responsible for the synthesis of archaeal membrane-spanning GDGT lipids. *Nature Communications*, *13*(1), 1545. https://doi.org/10.1038/s41467-022-29264-x

Zhu, Z., Wu, J., Rioual, P., Mingram, J., Yang, H., Zhang, B., et al. (2021). Evaluation of the sources and seasonal production of brGDGTs in lake Sihailongwan (NE China) and application to reconstruct paleo-temperatures over the period 60–8 ka BP. *Quaternary Science Reviews*, *261*, 106946. https://doi.org/10.1016/j.quascirev.2021.106946